The Pennsylvania State University

The Graduate School

Department of Electrical Engineering

AN OPTICAL DETECTION SYSTEM FOR A RAYLEIGH/RAMAN LIDAR

A Thesis in

Electrical Engineering

by

Tim D. Stevens

Submitted in Partial Fulfillment
of the Requirements
for the Degree of

Master of Science

August 1992

We approve the thesis of Tim D. Stevens.

Date of Signature

_____ _____

Charles R. Philbrick
Professor of Electrical Engineering
Thesis Advisor

_____ _____

John D. Mathews
Professor of Electrical Engineering

_____ _____

Chih-Chung Yang
Associate Professor of Electrical Engineering

_____ _____

Larry C. Burton
Professor of Electrical and Computer Engineering
Head of the Department of Electrical and Computer Engineering

ABSTRACT

The optical detection system and preliminary results of the new Rayleigh/Raman LAMP (Laser Atmospheric Measurement Program) lidar developed at The Pennsylvania State University are presented. The LAMP lidar was designed as a research instrument to investigate properties of the lower and middle atmosphere. The fabrication of the instrument hardware was sufficiently complete in June 1991 that initial testing of the instrument was begun. The instrument provides profiles of density and temperature structure of the middle and lower atmosphere, along with water vapor profiles of the lower troposphere. The design of this lidar will be described from an optical engineering point of view. The receiving system, shuttering system, optical processing, and light detection are all explained. Calculations of the expected performance for measurement of atmospheric properties have been considered in the engineering design so that the scientific goals are achieved. Examples of the results are presented to illustrate the capabilities of the LAMP lidar. Data examples have been selected from the first field trip in which the LAMP lidar operated aboard the German research vessel RV Polarstern as part of the LADIMAS (LAtitudinal DIstribution of Middle Atmospheric Structure) campaign. Measurements were taken from 70° N to 65° S between October 1991 and January 1992 aboard the German research vessel, RV Polarstern.

TABLE OF CONTENTS

LIST OF FIGURES

LIST OF TABLES

ACKNOWLEDGMENTS

I would like to thank my advisor, C. R. Philbrick, for teaching me the value of being a curious observer. I would also like to express my gratitude for his guidance and encouragement throughout the writing of this thesis. The committee members, J. D. Mathews and C. C. Yang, were most helpful with their support and recommendations.

Thanks are due to Yi-Chung Rau, Paul Haris, Subha Maravada, George Evanisko, Steve McKinley, and Glen Pancoast for their help and contributions to this thesis.

I would also like to thank DuPont and the ARL Exploratory and Foundational Fund (E &F) for their support of my graduate schooling.

The effort to prepare the LAMP instrument has been supported by PSU/ARL project initiation funds, Penn State College of Engineering, Laser Atmospheric Measurement program for the US Navy, and the National Science Foundation's CEDAR (Coupling Energetics and Dynamics of Atmospheric Regions) Program. The measurements on the RV Polarstern were made possible by invitation of the Alfred-Wegener-Institut, which is gratefully acknowledged. Collaborative efforts with Professors U. von Zahn and D. Offermann have made these investigations possible.

Chapter 1

INTRODUCTION

The ever-increasing questions concerning changes in our environment and global warming issues have caused us to search for better ways to monitor and model the atmosphere in which we live. We study the atmosphere not only to understand the structure and processes within it, but also to evaluate the effect of man's activity on the biosphere. The recent depletion of ozone in the Antarctic [7] and a steady increase in CO_2 concentration [21] are issues that raise public concern and motivate scientists to investigate atmospheric properties that were once thought to have only academic interests. Lidar (light detection and ranging) is one of the newest and most versatile techniques available for studying the atmosphere. Lidar provides profiles of density and temperature from 0 to 100 km [4], trace constituents (i.e. iron and sodium) between 80 and 120 km [3,8], water vapor in the troposphere [14], aerosols [20] and cloud extinctions, and many other atmospheric parameters. The idea of using the molecular scattering of light to investigate atmospheric properties was first explored by Elterman in 1951 with a searchlight [6]. In 1962, the development of the pulsed laser led to range resolved measurements of the backscatter intensity from particles and molecules of the atmosphere.

Lidar is similar to radar, except it uses light instead of radio waves. Short laser pulses, approximately 5 ns, are transmitted into the atmosphere and the backscattered light is collected by a photodetector. The time is measured between the transmitted and

received laser pulses, providing the altitude resolution. The integration time determines the range resolution of the atmospheric measurement. There are many types of scattering in the atmosphere which are of use to lidar. This paper will be concerned with the following three: Rayleigh - elastic molecular scattering where the scatterers are small compared to the wavelength of light, Mie - scattering by particles which are on the order of the wavelength of the incident radiation, and Raman - inelastic molecular scattering where the emitted photon will either gain or lose a discrete amount of energy specific to the vibrational energy states of the molecule [13].

Equation (1) is commonly called the lidar equation, and is used as a design guide

$$N(z) = \eta_{eff} T_A \times \frac{P_L}{hc/\lambda} \times \sigma_R n(z) \Delta z \times \frac{A_R}{4\pi z^2} \qquad (1)$$

in choosing many of the components which make up a lidar. There are four prime terms in the equation, which account for: 1) transmitting efficiency, 2) transmitted power, 3) scattering probability, and 4) receiving probability. Given the above parameters, it is then possible to calculate N(z), the number of scattered photons received from a particular height z. The instrument characteristics will be discussed here, while the scattering processes and results will be discussed in Chapters 4 and 5.

1.1 LAMP Background

Lidar techniques have been developed to measure a variety of atmospheric properties from molecular temperature to water vapor concentration [15], but no

previous lidar has been built to observe such a wide range of altitudes and atmospheric properties simultaneously. The LAMP instrument was designed to operate as both a middle atmosphere sensor and a lower atmosphere meteorological sounder. To accomplish this task, many parameters including nitrogen, water vapor, aerosols, density, and temperature must be monitored over large altitude ranges at the same time. The LAMP lidar utilizes molecular scattering (Rayleigh and Raman) and particle scattering at two wavelengths, 355 nm and 532 nm, to obtain the information needed to extend lidar temperature and density measurements through the troposphere and down to the ground [2,17]. Table I lists the atmospheric parameters and the corresponding altitude ranges measured by LAMP. A Fabry-Perot etalon with special built tuning electronics and narrow band-pass filters make daytime measurements possible. The LAMP instrument

Table I.
Characteristics of The Penn State LAMP lidar.

Lamp Characteristics
Temperature and density from 15 to 80 km.
Nitrogen profiles from ground to 20 km.
Aerosol two-color discrimination using 355 & 532 nm.
Temperature and density from 0 - 15 km.
Water vapor profiles from ground to 5 km.
Cloud characterization and profiling.
Daytime measurements to 50 km.

was also built as a test bed for the development of more advanced meteorological sensors capable of fully automated operation. The LAMP lidar is a self-contained transportable instrument capable of operating in almost any environment, as was demonstrated by its operation aboard the German ice breaker RV Polarstern in Antarctica during December 1991.

Design work on the LAMP lidar began in October of 1989 with the focus on building a transportable instrument capable of field measurements in all weather conditions. Construction and testing began by fall of 1990 and system testing started in June 1991. The instrument was relocated from the electrical engineering laboratory to a 20' x 8' x 8.5' container, which was used as a field laboratory during the summer of 1991. In September 1991 the lidar was shipped to Andenes, Norway, for its first measurement campaign. The field laboratory is a standard cargo shipping container which has been modified with doors, hatches, insulated walls and equipped with three 60 Amp multiple tap transformers, which enable the lidar to operate on almost any power system.

The LAMP instrument collected its first field data as part of the LADIMAS campaign on September 24, 1991, at the Andøya Rocket Range, Noway. The LADIMAS (LAtitudinal DIstribution of Middle Atmospheric Structure) experiment included ship-board measurements between 70° N and 65° S to study the structure, dynamics and chemistry of the atmosphere[19]. The campaign began with a period of testing and coordinated rocket measurements at the Andøya Rocket Range. The lidar was installed on the helicopter deck of the RV Polarstern at Tromsø, Norway on October 10, 1991. Several profiles of hazy low altitude atmospheric data were collected while in transit to

Bremerhaven, Germany. Measurements were obtained on every clear night aboard the RV Polarstern as it sailed on legs from Germany to Argentina, Antarctica and then to Chile.

The emphasis of this paper will be on the design of the optical instrumentation of the LAMP lidar. As an introduction to the design problem, an overview of the five subsystems of the instrument will be presented: transmitter, receiver, detector, data system, and control/safety systems.

1.2 LAMP Instrumentation

The subsystems of a lidar are the transmitter, receiver, detector, data system, and control/safety systems. The LAMP system uses a 20 Hz pulse repetition frequency Nd:YAG laser transmitting 1.5 joules per pulse at 1064 nm. The fundamental output energy is doubled and tripled by nonlinear crystals to produce outputs at wavelengths of 532 nm and 355 nm. Table II provides a summary of parameters for the LAMP lidar. The wavelengths and altitude ranges of each of the six independent photodetectors are shown in Table III. Each channel is either digitized or photon counted depending on the intensity of the signal and the dynamic range needed for that altitude range. Figure 1 shows the Penn State ground-based LAMP lidar in a schematic overview. The system design is an advanced development from two earlier lidars, the GLINT and GLEAM systems developed by Philbrick at the Air Force Geophysics Laboratory (currently Phillips Laboratory) [17,18]. The subsystems shown in Figure 1 include the transmitter,

Table II
Penn State lidar parameters.

PENN STATE LAMP LIDAR PARAMETERS			
Power Aperture product = 1.55			
TRANSMITTER			
Type: Continuum NY-82, Seeded Nd:YAG			
	Fundamental	Doubled	Tripled
Wavelength	1064 nm	532 nm	355 nm
Pulse Energy	1.5 J	600 mJ	250 mJ
Bandwidth		80 MHz	
Pulse length		6 ns	
Pulse rate		20 Hz	
RECEIVER			
Type: f/15, Cassegrain Telescope			
Focal Length		609 cm	
Primary Diameter		40.6 cm	
Secondary Diameter		10.2 cm	

Table III
Six independent detector channels of LAMP

Detector Channels
532 nm high altitude (15 - 80 km), photon counting
532 nm low altitude (200 m -15 km), digitizing
355 nm high altitude (15 - 80 km), photon counting
355 nm low altitude (200 m -15 km), digitizing
607 nm N_2 Raman (200 m - 25 km), photon counting
660 nm H_2O Raman (200 m - 5 km), photon counting

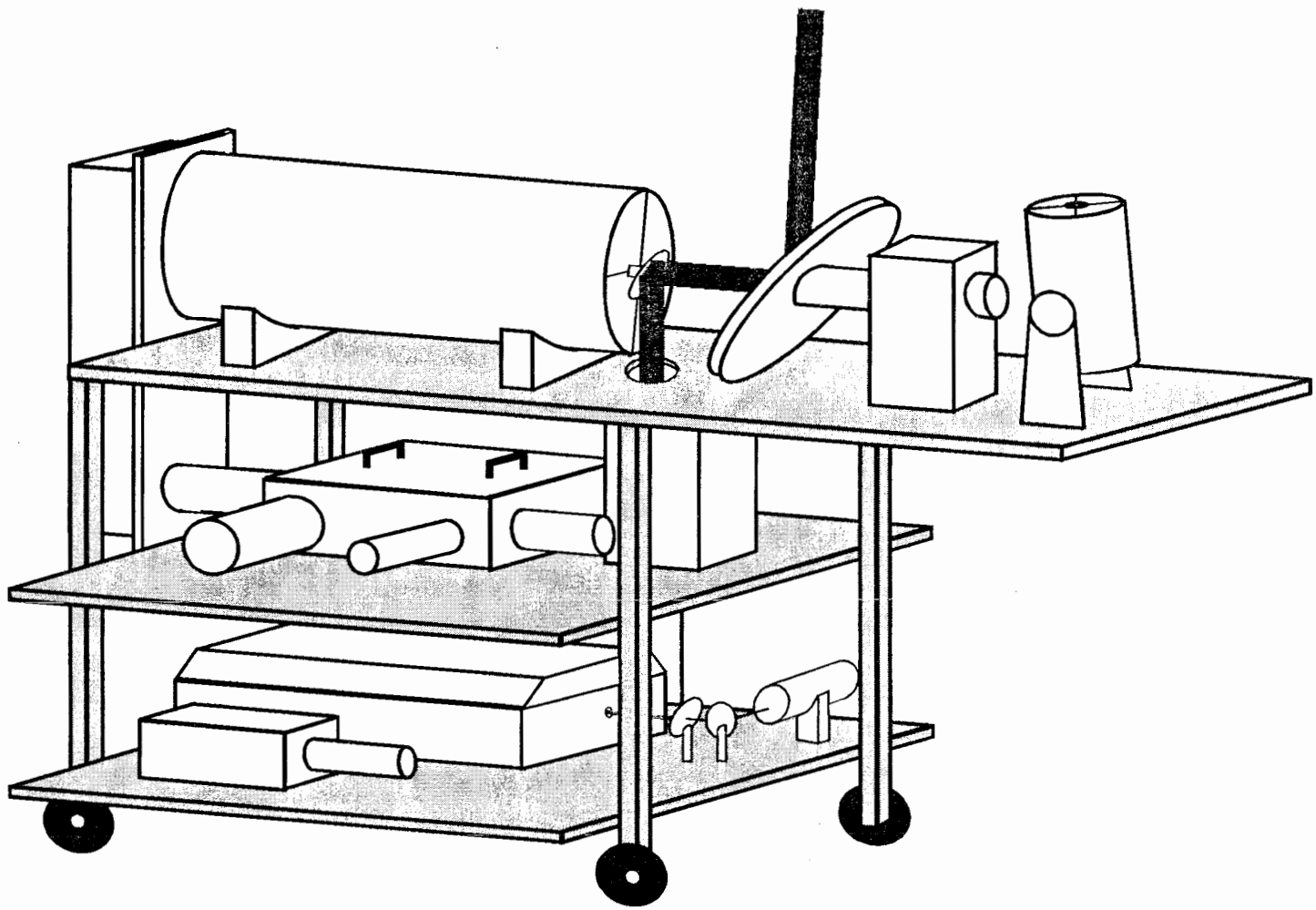

Figure 1. Drawing of the LAMP instrument and three of its five subsystems: transmitter, receiver and detector.

located on the bottom of the table, the receiver, located on the elevated shelf of the table, and the detector section on the primary working level of the table. The dimensions of the table are 9 ft. long, 7 ft. high, and 4 ft. wide, which enables it to easily fit in a standard shipping container and allows room for the data system and other supporting instruments, i.e. safety radar. The table is equipped with wheels, which are placed in rails, so it can be rolled to position the mirror outside through a window of a laboratory or a hatch of the field container to take measurements. The laser is located on the bottom of the table along with the laser pulse energy monitor and a secondary detector section. The laser beam is directed by a hard coated mirror through the second level of the table into a 5X beam expander. After being expanded, the laser beam is reflected off two hard coated mirrors and directed into the atmosphere. The backscattered light is collected by two receiving telescopes, a 40 cm classical Cassegrain, and a 20 cm Schmidt Cassegrain. A 61 cm receiving flat directs the field of view of the 40 cm telescope upward allowing the telescope to be positioned horizontally. This design allows the lidar to scan in a vertical plane simply by rotating the 61 cm flat, and enables the lidar to measure through a side window instead of a roof opening. The received light is collimated, and beam forming optics direct the received light from the telescope into the detector box where it is separated in six different signal channels. A secondary 20 cm receiving telescope is used for overlapping data through the 8 - 35 km altitude region. The light received by this telescope is guided by a fiber optic cable into a secondary detector box where it is optically processed and detected by one of three different photomultiplier tubes (PMT's). The PMT signals are converted from current pulses to either voltages for digitizing, or to

NIM level signals for photon counting. These signals are recorded by a data system made up of in-house built electronics and CAMAC data acquisition modules. A Zenith 386 PC saves the data to a 1 GByte WORM optical disk.

The emphasis of this paper is on the optical detection system of the lidar and is shown as a block diagram in Figure 2. Three primary optical sections will be addressed in the order of the light signal path through them. First, the receiving optics collect the backscattered light and prepare it to be guided into the shuttering section. Second, the shutter allows only light from certain altitudes to reach the PMT's. Next, the optical processing branch is divided into two sections, light discrimination and light detection. The light discrimination branch divides the light in three paths to be shuttered, optically discriminates according to wavelength, and allows only light of certain wavelengths to illuminate the photodetectors. Finally, the photocathodes of the PMT's in the light detection branch convert photons to electrons, which are then subject to a gain of 10^6 to 10^7 using an avalanche gain technique. These three sections complete the optical portion of the lidar, everything after the light detection stage is dealt with electronically. The electronics and data acquisition logic will be addressed in Appendix A.

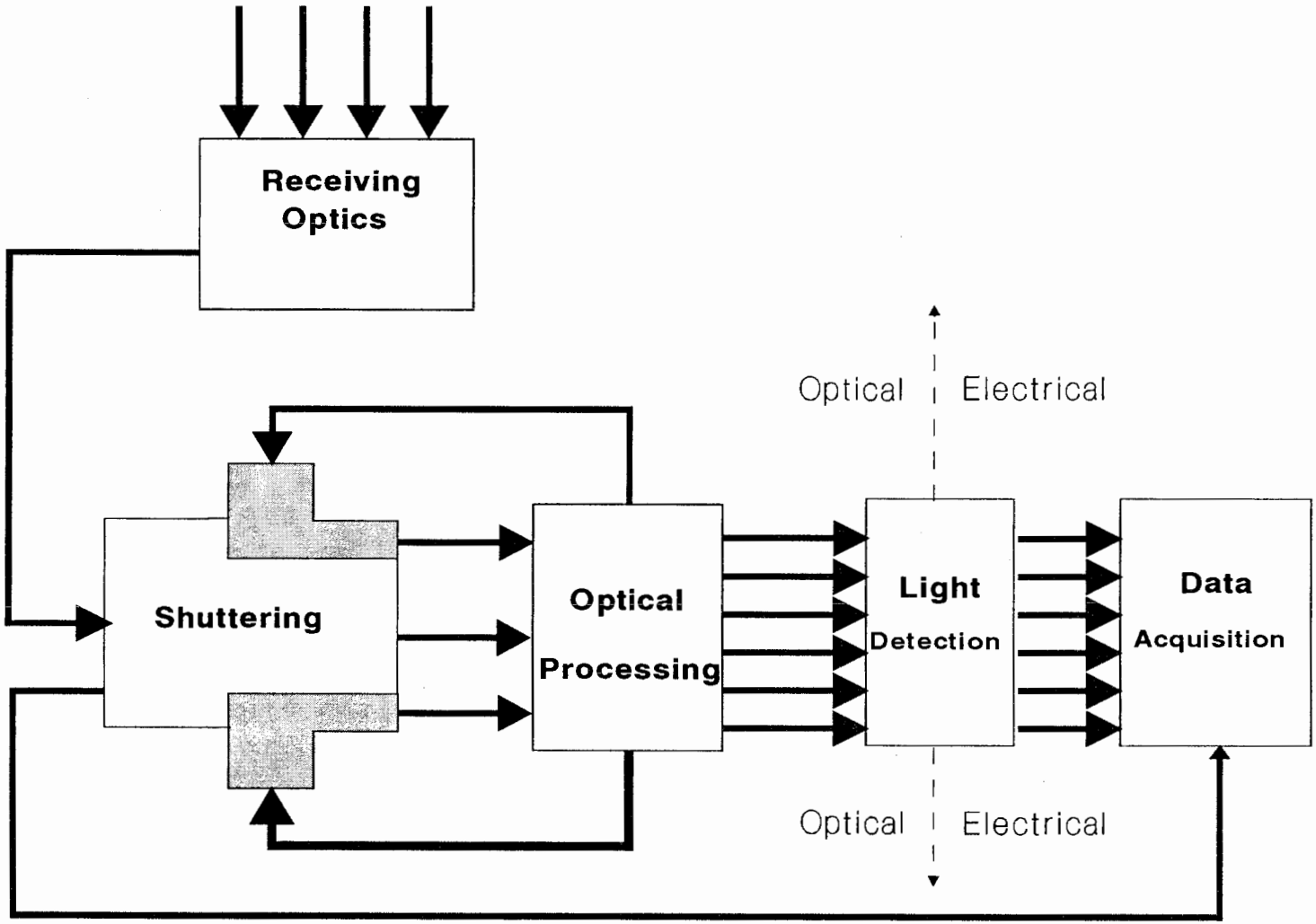

Figure 2 . Optical block diagram of the LAMP lidar.

Chapter 2

RECEIVING OPTICS

The first optical component of any lidar is the receiving system. A block diagram of the LAMP receiving setup is shown in Figure 3. At the center of the LAMP lidar receiving system is a 40 cm Dall-Kirkham telescope with a 609 cm focal length. The telescope is positioned on its side as shown in Figure 4, and a 61 cm optical flat is used to direct the field of view of the telescope upward. Positioning the telescope on its side accomplishes two goals; it makes the system more portable and compact, and prevents the telescope from collecting dust. The 61 cm mirror will also rotate on its center axis so the system's field of view can be manually steered. The backscattered light collected by the telescope is focused about 15" behind the primary mirror and is directed, by a 2" mirror, down to the field stop, as shown in Figure 4.

The field stop is the first of three optical elements that prepare the light for shuttering and optical processing. Reduction of the background signal is very important for daytime and for high altitude lidar measurements, and limiting the field of view is one way to significantly increase the signal-to-noise. A field stop is placed at the primary focus of the telescope and adjusted to limit the field of view to about two times the laser's diameter at 90 km. The placement of the field stop is critical, if it is not located exactly at the primary focus of the telescope it will begin to act as an aperture stop which reduce the total amount of light collected over the full field of view. When photon counting, all backscattered laser light is valuable, so care must be taken in positioning the field stop.

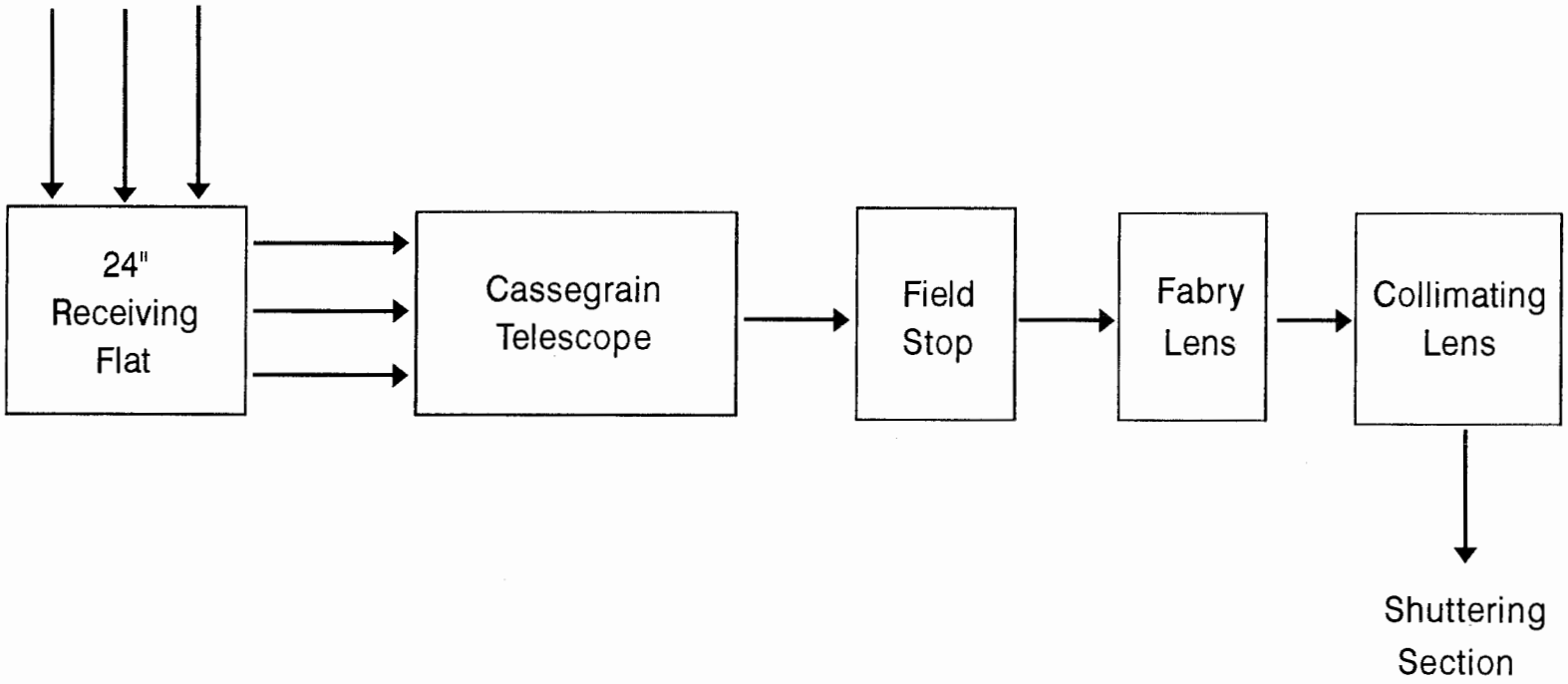

Figure 3 . Block diagram of the receiving optics section. Five optical components collect the backscattered return from the atmosphere and form it into a collimated beam for shuttering and optical processing.

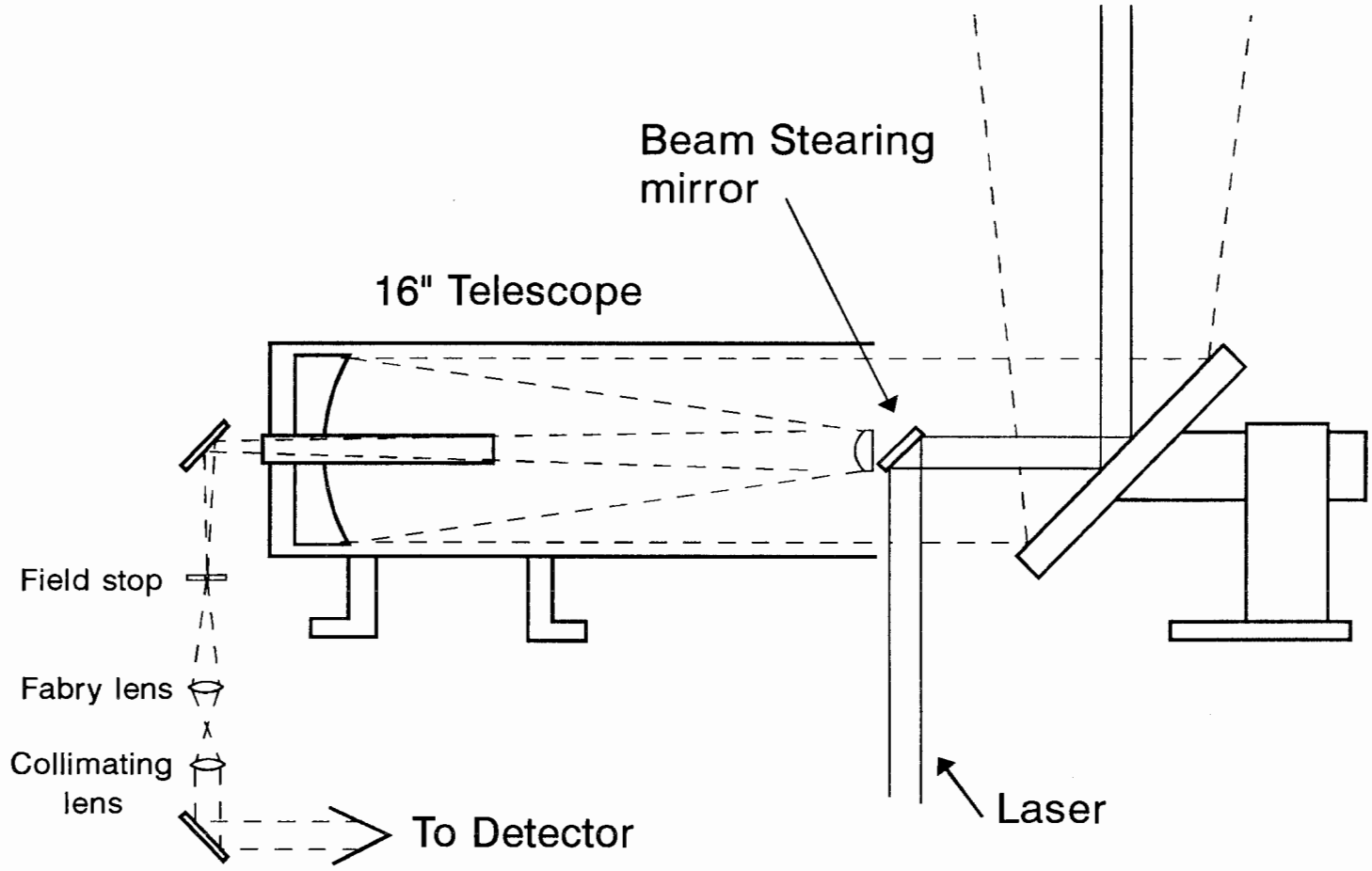

Figure 4 . Drawing of the optical ray path through the receiver system. The position of the field stop and following two beam forming lenses is shown with respect to the 16" Cassegrain telescope and 24" collecting flat.

A typical diameter used for a field stop would be 1 mm.

The next component in the receiving section is the Fabry lens. There is nothing special about the lens itself, only the way it is used. Without a Fabry lens the collimated light being processed would contain a direct image of the laser, and would show up as a bright spot centered in the telescope field of view. Figure 5 shows what the beam would look like on a white card with and without a Fabry lens. There are two problems with this bright spot. When shuttering the light, it takes a small amount of time for the shutter to pass through the beam. If the beam is not uniform no useable information can be gathered during the shuttering process, only after the shutter is fully open. Second, Photodetectors will respond more linearly to a uniform light intensity than to a "hot" spot on the center of the detector. A one inch bi-convex lens is used as the Fabry lens and placed so it images the primary mirror of the telescope, see Figure 6. Light incident on the primary mirror is uniformly distributed and has not yet formed an image. Only the intensity or number of photons is important not the actual image. Using simple lens equations the position of the Fabry lens can be calculated. Once the lens is placed according to the calculation, it can be adjusted more critically by looking for the spider image at the focus of the lens with a white card. It should be noted that the Fabry lens can be placed either before or after the primary focus of the telescope. However, if it is placed before the primary focus, positioning of a field stop becomes significantly more complicated.

One rule must always be remembered when processing light with simple lenses, the area of the focused beam multiplied by the incident angle will always remain a

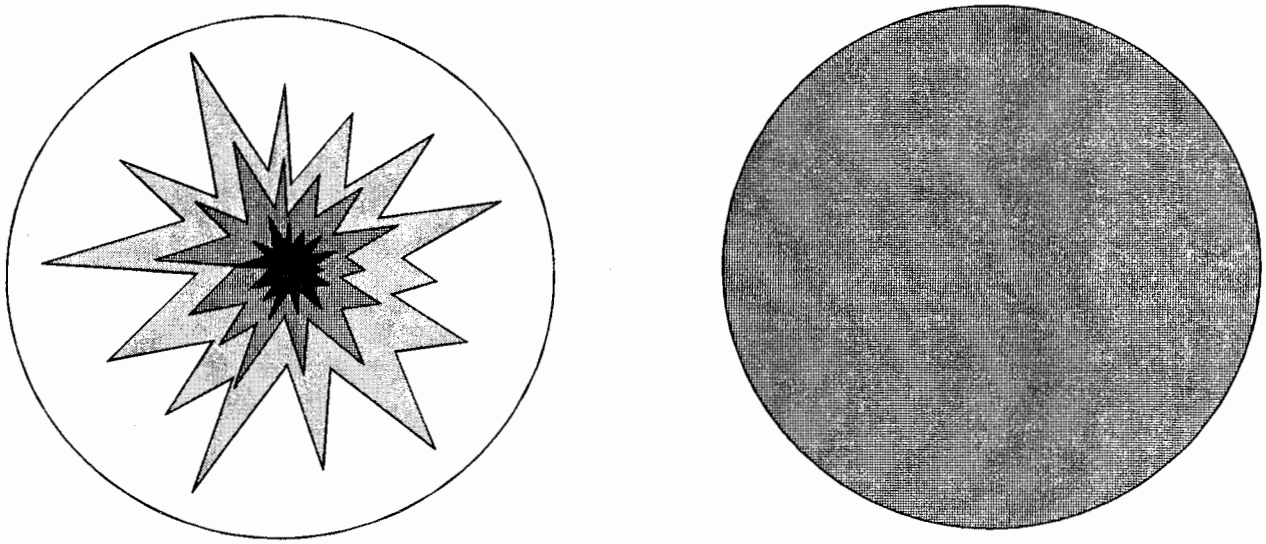

Without Fabry lens

With Fabry lens

Figure 5 . Cross sectional view of the backscattered light beam on a white card. Without the Fabry lens in the system, the center of the beam is very bright and the energy is not evenly distributed throughout the field.

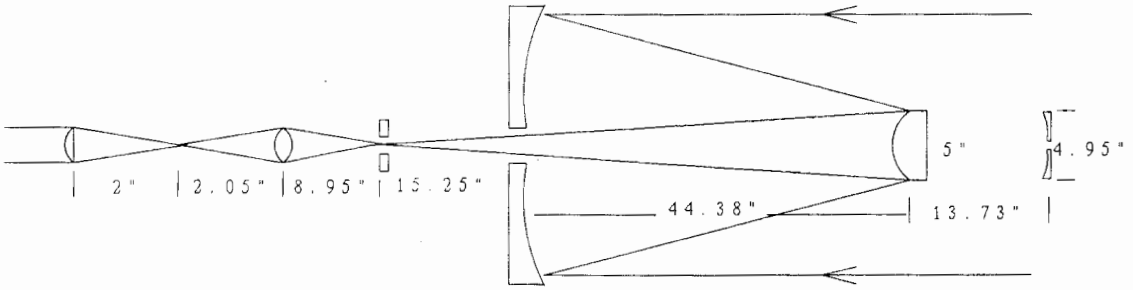

Figure 6. The Fabry lens position shown together with the marginal rays in the telescope system.

The primary mirror image is located at:

$$\frac{1}{S_i} = \frac{1}{S_o} + \frac{1}{F'} \tag{2}$$

The primary mirror focal length is 60" and the secondary mirror focal length is:

$$F' = \frac{B}{m-1} = S_o \tag{3}$$

Where m is the telescope magnification, and:

$$F' = \frac{59.63}{4 - 1} = 19.88 \ \textit{inches} \tag{4}$$

$$S_o = 44.38, \quad B = 15.25 + 44.38 \tag{5}$$

$$\frac{1}{S_i} = \frac{1}{44.38} + \frac{1}{19.88} \tag{6}$$

$$S_i = -13.73 \ \textit{inches} \tag{7}$$

The magnification of the primary image is:

$$M = \frac{S_i}{S_o} = \frac{13.73}{44.38} = .3094 \tag{8}$$

The height of the image is:

$$Y_i = 16 \times .309 = 4.95 \ \textit{inches} \tag{9}$$

constant, $A \cdot \Omega$ = constant, for each element of an optical system. This means, the closer the focal plane is to the lens, the smaller the focal point will be. When trying to collimate a point of light it is important that the spot size be as small as possible. A positive lens will perfectly collimate the light from an infinitely small object, but as the object moves off-axis, the cone of rays that can reach the image plane become narrower. This is an effective aperture stop that limits the amount of light that can reach the image plane. The result is a gradual fading out of the light beam near the edges, a process known as vignetting [10].

Using the Gaussian lens formula, both the position of the Fabry lens and the collimating lens can be calculated. First, the Fabry lens must be placed as far from the primary focus as possible. This is so the focal point of the Fabry lens will be as small as possible (remember the rule from above). By keeping the Fabry lens far from the primary focus, a large angle is obtained, thus minimizing the spot size and making it easier to collimate the light. To minimize spherical aberrations and to contain the marginal rays within the system, the Fabry lens is placed such that the incident light covers only 75% of its diameter. Next, the size and location of the virtual image of the primary from the secondary is calculated. This virtual image is focused by the Fabry lens, and its focal distance calculated. The same calculation is worked out for the focal point of the primary focus from the Fabry lens. These foci turn out to be separated by about 0.5", which is sufficient to collimate only the primary image. Placing the collimating lens is now easy, the lens should be positioned one focal length from the focal point of the Fabry lens. Now that we know the focal point of the primary mirror is located 2.05"

from the Fabry lens and the primary focus is located 2.58" away from the Fabry lens, the collimating lens should be placed 4.05" away from the Fabry lens, thus collimating only the primary image. See Figure 6. Since the image from the primary focus is inside the focal length of the collimating lens, its image will not come to a focus again, and therefore will not be processed through the system. The light is formed into a 0.73" diameter collimated beam, which is shuttered. It is worth noting that the light is never perfectly collimated with any optical system and there is a constant struggle in design of a long path length to keep the light from aperture loss outside the optical components. Extra lenses are added at various places to focus the light back into the correct optical path.

Chapter 3

SHUTTERING SYSTEM

An important optical component in the LAMP lidar is the optical shutter. A typical return through the Earth's atmosphere falls off nine orders of magnitude between 1 and 80 km. This large dynamic range makes it impossible to monitor the backscattered return with one detector. A photodetector sensitive enough to detect the small return at 80 km will be saturated by the large signal near the Earth's surface; therefore, a multi-element detection system is required. The high altitude detector must not be exposed to the return signal from the lower atmosphere. There are two methods for protecting the PMT's (Photomultiplier tubes) from saturation. One method is to gain switch the PMT so that it is not turned on until sometime after the laser has fired. However, there are problems with this approach because the PMT will usually not settle and respond linearly until many milliseconds after it has been turned on, and also the photocathode behaves in a non-linear fashion after a strong signal is applied. A second method is to use a mechanical chopper wheel that closes when a large signal is returning from the lower atmosphere and opens when a weak signal is returning from the upper atmosphere. This is the method used by the LAMP lidar and will be discussed here.

The LAMP lidar was designed to operate through the troposphere as well as in the mesosphere, this required a shuttering system that blocked out the first few kilometers for low altitude measurements and blocked out the first 10 - 20 km for high altitude measurements. Dual shuttering was needed, but two chopper wheels would pose a

difficult problem because of the critical synchronization between them. A unique solution is to pass the light through the optical chopper once to block everything below 3 km, then send 1 % of that light signal to be processed as low altitude return. The other 99 % would be sent back through different openings of the same chopper to block out the lower 20 km, this signal would then be processed as high altitude return. Figure 7 details the optical paths as described above. The signal from the telescope is sent through one opening of the chopper, and the firing of the laser is timed so the first 3 km of the return is blocked. The signal returning from 3 - 80 km is split into 355 and 532 nm wavelengths and narrow band filtered. Approximately 1% of each of these wavelengths is directed to a low altitude detector; the other 99% is sent to be optically shuttered again. Both the 355 and 532 nm signals are sent back through the same chopper on two separate paths. This pass is timed to block out all return up to 20 km, and is processed for high altitude return. Finally, the chopper wheel closes the light path at an equivalent altitude of about 80 km.

Figure 8 shows a drawing of the LAMP chopper wheel and all its openings. The chopper is fourfold symmetric, allowing more openings per revolution and permitting the balancing of the wheel for high velocities. There are two sets of openings, an inner diameter for shuttering out the first 3 km and an outer diameter for the second pass to block out the lower 20 km. Three dots on Figure 8 indicate the locations where the light is focused onto the surface of the chopper wheel. Point (1) is the location where all wavelengths of light are shuttered to block out the first 3 km. Both points (2) and (3) are placed so they are shuttered at the same time due to the symmetry of the chopper wheel.

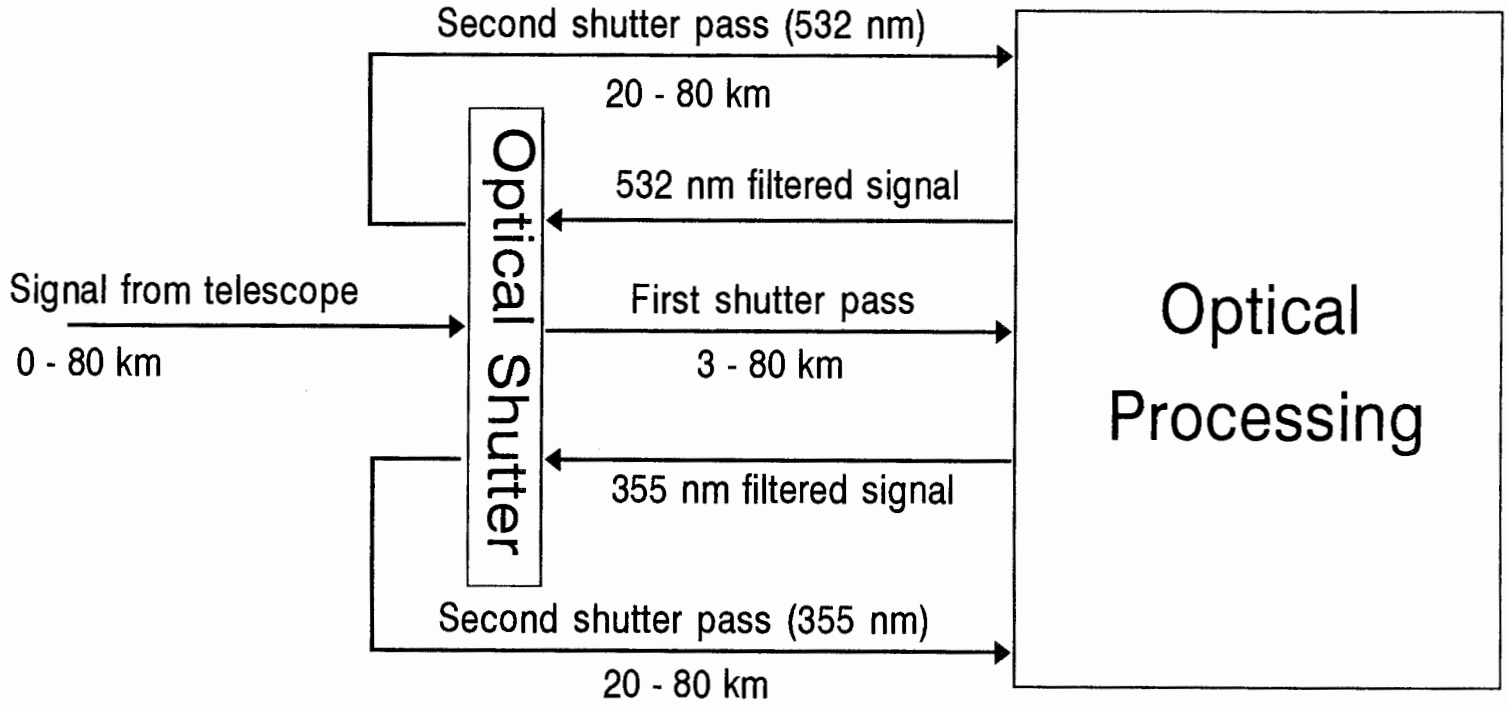

Figure 7 . Shuttering block diagram for LAMP showing the multiple light paths through the chopper. One chopper wheel shutters the light for two separate altitude ranges.

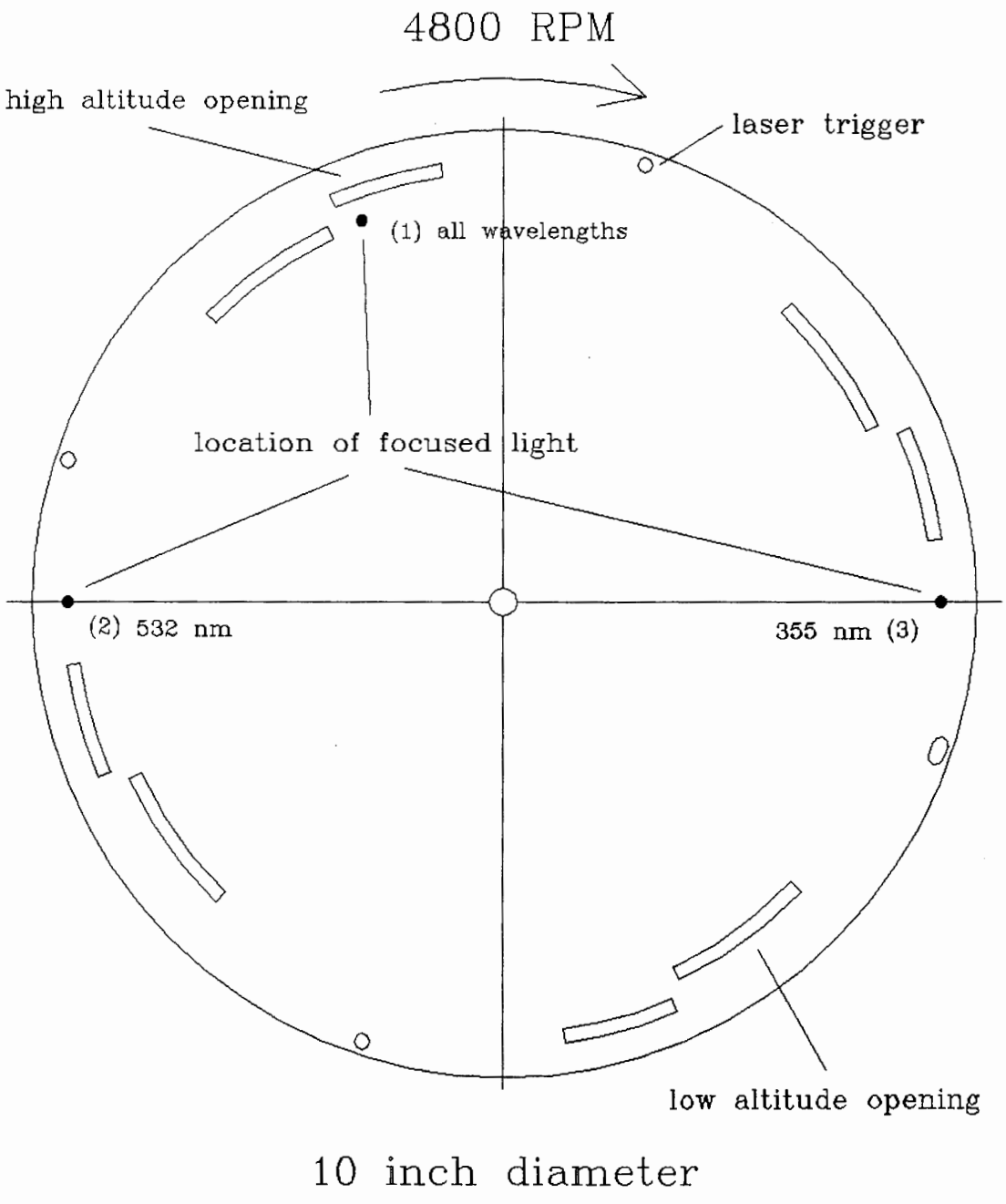

Figure 8. CAD drawing of the LAMP chopper wheel viewed from the front as the light would be entering the page. The chopper is fourfold symmetric with two sets of openings for multiple shuttering altitude ranges.

Because of the high velocity of light, the chopper wheel must rotate as fast as possible in order to open and close the shutter sharply. Due to the design of directing three focused light paths onto the same chopper wheel, the wheel had to be at least 10 inches in diameter. This limited the velocity at which the wheel could rotate. The practical limit for a precision machined aluminum wheel was about 5000 rpm (as was discovered by experiment). A different light weight material would have to be specially machined to avoid resonance above 5000 rpm. The position of the chopper wheel at the firing of each laser pulse is critical to the performance of the system. Each laser shot must be triggered by the chopper wheel to ensure that the chopper is positioned properly with respect to the laser return. This is accomplished by a small hole drilled in the chopper, symmetric with the high and low altitude openings (Figure 8). A small photo-diode detector/emitter is placed on either side of the chopper to provide a signal for initiating all triggers for the lidar system. It would be impossible to perfectly machine the chopper so that all openings were placed exactly symmetric to each other; therefore, one trigger hole is elongated providing a master starting point for all measurements. The final rotation speed of the chopper should be a multiple of the repetition rate of the laser. The laser will Q-switch most efficiently at a repetition rate of 20 Hz, so the master laser trigger on the chopper must make at least one revolution every 50 msec. The chopper must also rotate as fast at a high speed so the "on-off time" of the focused point of light is as short as possible. A velocity of 4800 rpm allows a laser fire every 16 shutter openings corresponding to 20 Hz. One shutter opening is allotted for the laser return, 14 shutter openings are allocated for background measurements and one opening period is

used to record the laser energy. All 16 measurements are recorded during the 50 msec period. Once the velocity of the chopper was determined, the exact position of the openings could be calculated.

The time it takes the chopper to go from fully closed to fully open is important so that a minimal amount of data is lost in the transition. If the chopper opens too slowly it is possible for a cloud return to saturate the photodetectors while the shutter is opening. This is because the return signal from a cloud is much stronger than the molecular return from the atmosphere. The time the chopper takes to open is a function of the size of the focused light point on the chopper, the diameter of the chopper and the velocity of the chopper. The LAMP chopper wheel is 10" in diameter and rotates at a velocity of 4800 rmp. See Figure 8. The focused spot of light on the chopper's surface was calculated to be 1.68 mm in diameter. Using these figures, simple geometry calculations show that the chopper should transit from fully closed to fully open in a time equivalent to 3.8 km. Figures 9 and 10 show a day-sky return through the system for both 355 and 532 nm wavelengths collected in Antarctica on December 23, 1991. The high altitude shutter was set to start opening at 10 km, and due to the length of the opening it at about 80 km. From this data it can be seen that the shutter is fully open by 14 km for the 532 nm channel and by 15 km for the 355 nm channel. Therefore the chopper is opening in 4 - 5 km which is very close to the calculated result. The 532 nm channel opens slightly faster than the 355 nm channel. This is probably due to chromatic aberrations causing the 355 nm wavelength to focus before the surface of the chopper. If the light focuses before or after the chopper's surface, the spot illuminating the chopper will be slightly larger and it will take longer for the chopper to go from fully closed to fully open.

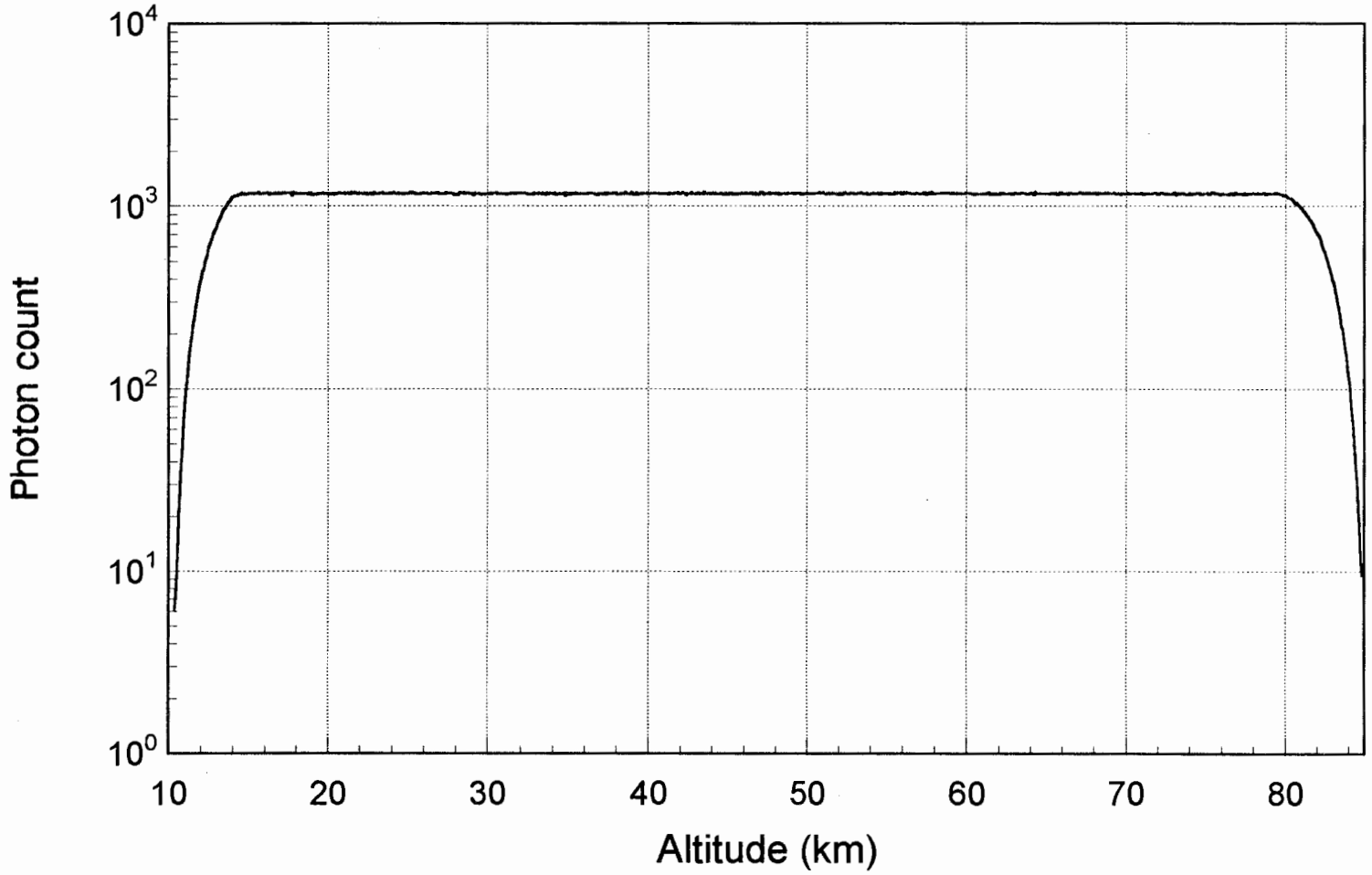

Figure 9. High altitude shutter response for the 532 nm channel. This data was collected from day-sky backgroud to show the opening and closing altitudes of the shutter.

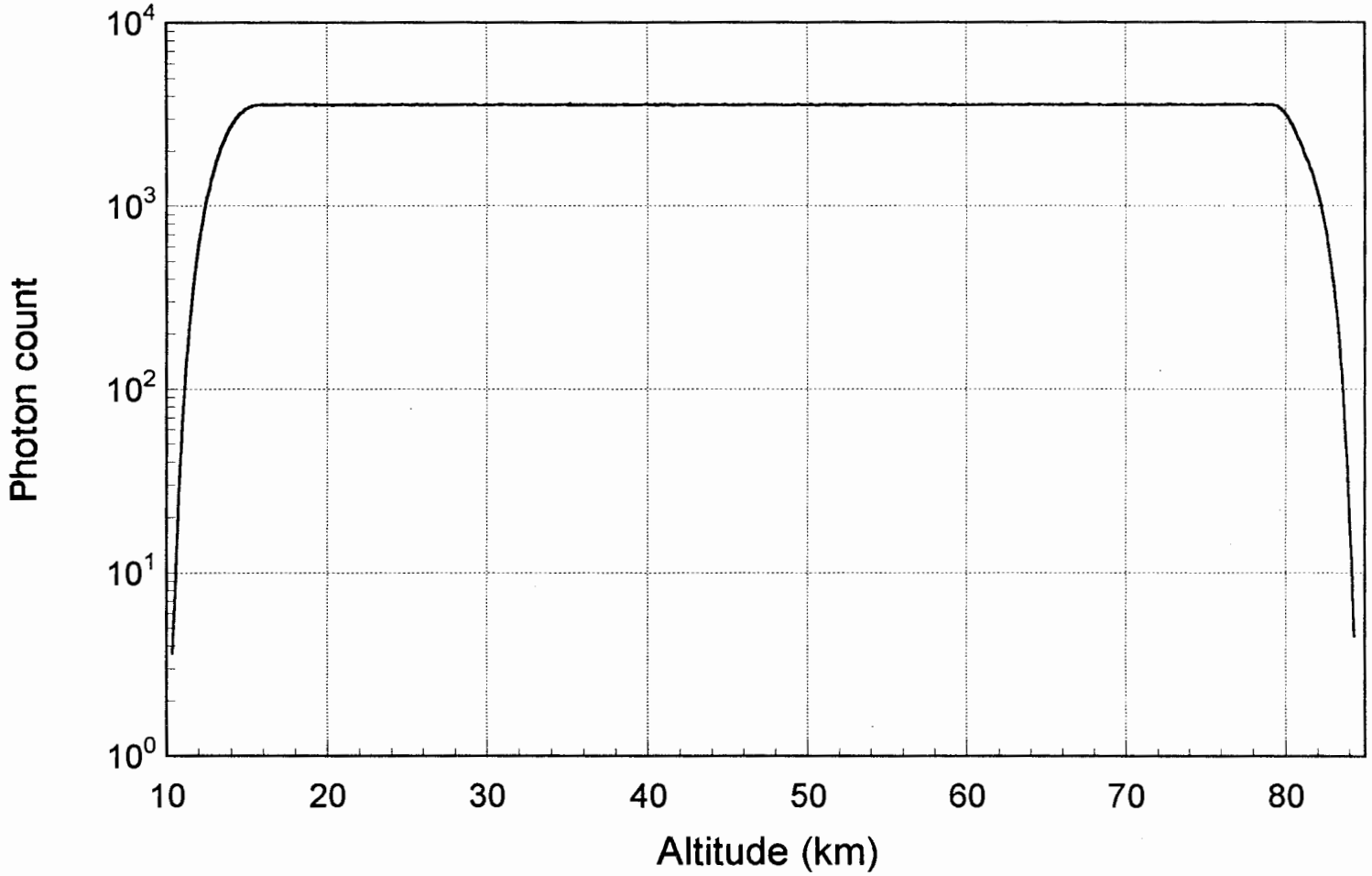

Figure 10. High altitude shutter response for the 355 nm channel. This data was collected from day-sky backgroud to show the opening and closing altitudes of the shutter.

Chapter 4

OPTICAL PROCESSING

It is the last major optical component, the optical processing branch, that defines the several important characteristics of a lidar. Once the laser energy is transmitted into the atmosphere there are several types of interactions that may be observed and recorded with the instrument, so decisions must be made concerning the science goals and atmospheric properties that will be monitored with the system. The LAMP instrument was designed to operate as both a middle atmospheric sensor and a lower atmospheric meteorological sounder. The lidar is therefore required to measure many more parameters than any previous lidar, making the optical processing branch more complicated. Previous lidars were concerned only with middle atmospheric temperature and density, or mesospheric iron and sodium layers[1,11]. The LAMP instrument monitors nitrogen and water vapor concentration, aerosol distribution and concentration, cloud characteristics, and middle atmospheric temperature and density simultaneously. Measuring mesospheric temperature requires only one photodetector and very few optical components, making the detection very efficient and enabling measurements to high altitudes. LAMP uses six photodetectors and many optical components, making the instrument more versatile but slightly less efficient for high altitude detection.

The optical processing is divided into two sections, optical discrimination and optical detection. Optical discrimination deals with splitting the light into its different frequency components, and focusing and directing it to the proper photodetectors. The

optical detection section explains the type of photodetectors used, their quantum efficiencies, and details of detection system.

4.1 Light Discrimination

Before an optical block diagram can be understood, an explanation of what optical wavelengths are being detected and why, must be presented. There are many types of scattering techniques utilized by lidars, Figure 11 indicates two of them in a schematic representation of Rayleigh and Raman scattering. Rayleigh scattering is an elastic scattering from molecules where no frequency shift is observed. LAMP transmits both 355 and 532 nm, therefore, a detection branch built to observe Rayleigh scattering from atmospheric molecules would measure the backscatter radiation at 355 and 532 nm. The LAMP lidar measures Rayleigh scattering to monitor both molecular temperature and density. Raman scattering is an inelastic scattering from molecules where a frequency shift characteristic of the molecule ($h\nu - nh\nu^* = E$, $h\nu^*$ represents the energy shift of the "n" vibrational energy states for stokes transitions) is observed. Every molecule has several specific vibrationally excited levels representing discrete shifts in the wavelength of scattered light. LAMP observes nitrogen and water vapor using the Raman scattering technique. When nitrogen is illuminated with laser energy at a wavelength of 532 nm, it will Rayleigh scatter at 532 nm and Raman scatter at 607 nm, likewise nitrogen will shift 355 nm to 387 nm. However, the scattering cross section of Raman scattering is about three orders of magnitude less than that of Rayleigh scattering. The same scattering

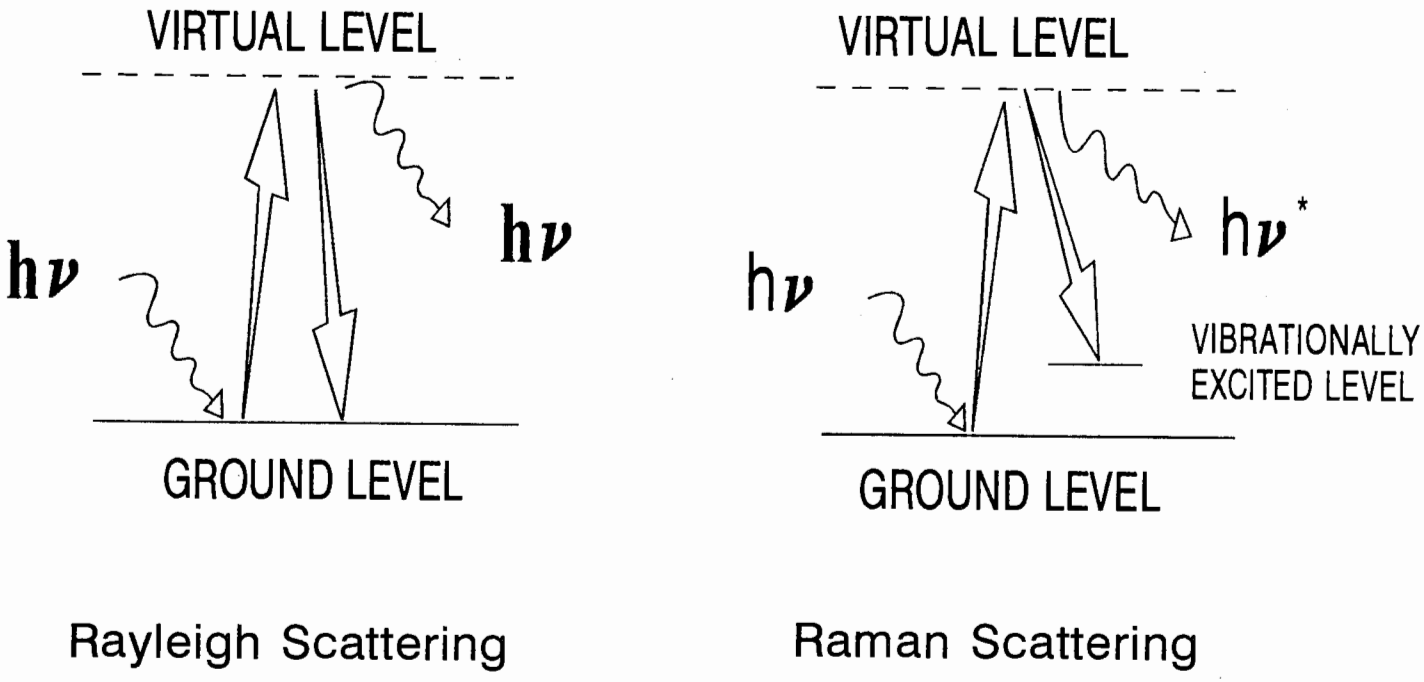

Figure 11 . Two molecular scattering techniques utilized by lidar. Rayleigh scattering is elastic scattering with no observed frequency shift. Raman scattering is inelastic scattering where a frequency shift characteristic to the vibrational energy states of the molecule is observed.

technique applies to water vapor, incident wavelengths of 532 and 355 nm are shifted to 660 and 408 nm respectively[5,15]. LAMP includes detector branches to observe both nitrogen and water vapor Raman shifts from 532 nm, although the Raman shifts from 355 nm could just as easily be monitored. Now that the reasoning behind why certain wavelengths are detected has been explained, a description on how these wavelengths are detected follows.

Figure 12 shows a block diagram detailing the optical processing branch of the LAMP instrument. The light enters this branch from the receiver section and is indicated in Figure 12 as the signal from the telescope. A series of two plano-convex lenses recollimate the light and focus it to a small spot onto the optical shutter. Plano-convex lenses are used so the refractive power of the lens can be shared between the two surfaces. Because optical efficiency is important, all lenses are AR (anti-reflection) coated for the wavelengths incident on their surfaces allowing 99.7 % transmission. All lenses require AR coatings for the four wavelengths; 355, 532, 607, and 660 nm. The light is collimated after passing through the shutter, and a beam-splitter with dichroic properties reflects 99.5 % of 532 nm and transmits approximately 85 % of 355, 607, and 660 nm. The path of the 532 nm light will be examined first.

To reduce background noise as much as possible, very narrow band-pass interference filters must be used. These filters use multiple layers of coatings to reduce the bandwidth of light allowed to pass, which decreases the transmission of the filter and makes them susceptible to band-pass shifts due to small temperature variations. A temperature stabilized housing is used to control the temperature of the narrow band-pass

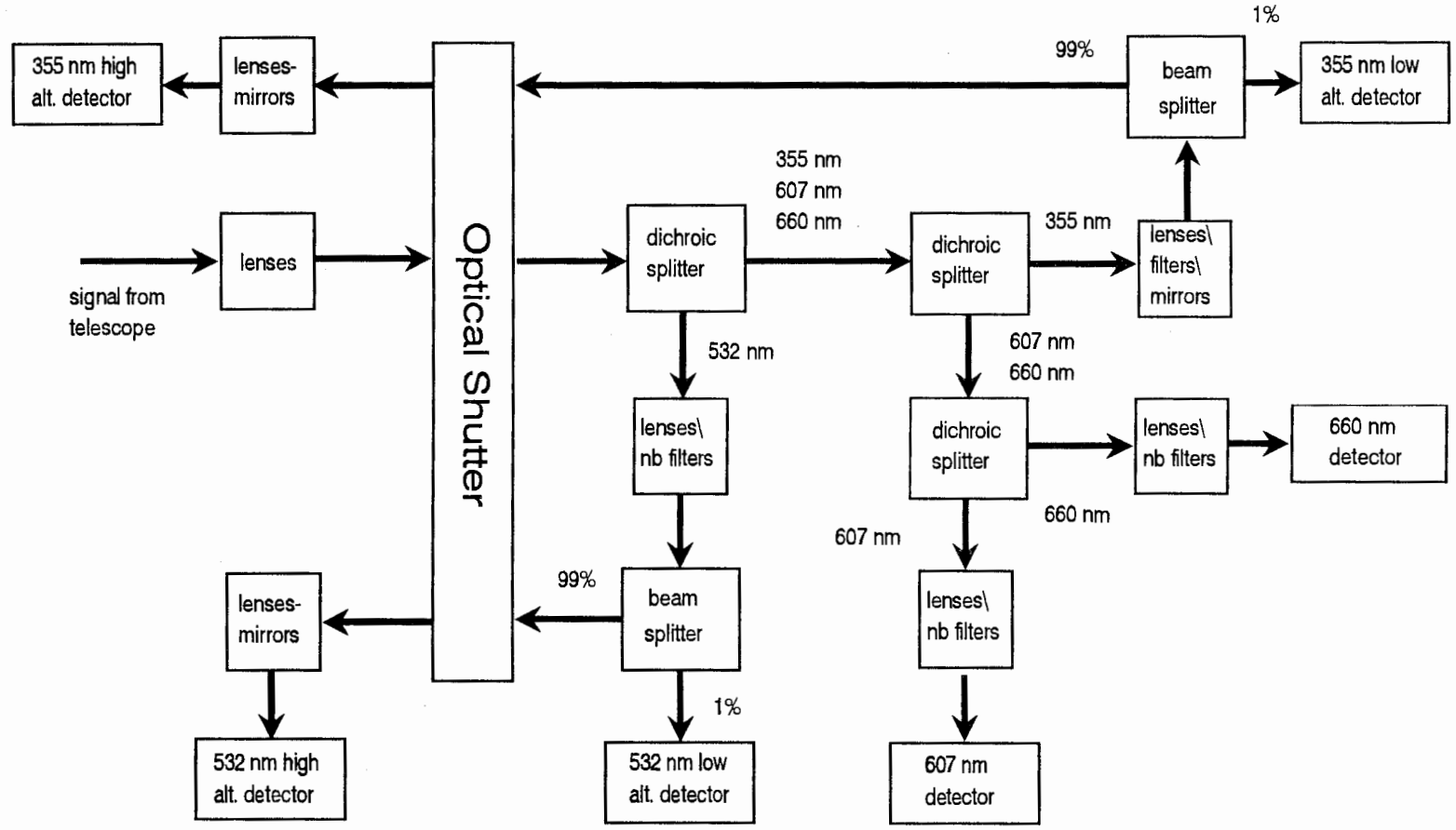

Figure 12. Optical processing block diagram showing the light paths through the lenses, filters, mirrors and beam-splitters. A total of six detectors are used to cover the appropriate spectral region over a wide dynamic range.

filters to 34° C +/- .1° C. The 532 nm interference filter has a bandwidth of 0.3 nm and 55 % transmission. Daytime measurements require even more drastic measures to reduce the background to an acceptable level. A removable Fabry-Perot etalon with a bandwidth of 0.01 nm centered at 532 nm is inserted before the interference filter for daytime measurements, it is tuned with special built electronics. Now that all wavelengths have been filtered out except for 532 nm, the light flux is ready to be directed onto the detectors. The low altitude detector needs only a small fraction of the light to obtain a large signal-to-noise ratio from the lower atmosphere. A beam-splitter transmits 1 % of the light to a low altitude detector and reflects 99 % to the shutter path of the high altitude detector. As discussed in the previous section the shutter removes all the light from below 20 km. A plano-convex lens focuses the light onto the shutter wheel and a similar lens recollimates the light after the shutter wheel. Both of these lenses need only be AR coated for 532 nm. The light flux is then directed onto the active area of the photo-detectors, which measure 9 mm in diameter. The light is focused at a point behind the detector's surface, such that the beam illuminates about 75 % of the surface.

After the first dichroic beam-splitter about 85 % of the 355, 607, and 660 nm light is incident on the second dichroic beam-splitter. This beam-splitter transmits 82 % of 355 nm and reflects 99.5 % of 607 and 660 nm. The reflected path of the 607 and 660 nm signal will be discussed next. A third dichroic beam-splitter separates the 607 nm light from the 660 nm light. The return from the Raman scattered 607 and 660 nm is relatively weak compared to the Rayleigh return, so altitudes of only 25 km for N_2 and 5 km for H_2O can be obtained. Because the 607 and 660 nm light is from Raman shifted scattering

of nitrogen and water vapor, its signal is about three orders of magnitude less than the signal from molecular scattering at the fundamental wavelength. Additionally, the Raman signal may be several more orders of magnitude less than the scattering from particles and aerosols in the lower atmosphere. The narrow band-pass filters that select these wavelengths must have very strong blocking characteristics at 532 nm. Both the 607 and 660 nm filters have a bandwidth of 3.5 nm, a transmission of 83 %, and a rejection at the laser line (532 nm) of 10^{10}.

Finally 85 % of the 355 nm wavelength is transmitted by the first dichroic beam-splitter. A narrow band-pass filter with a bandwidth of 3.2 nm, and a transmission of 24 % selects only the 355 nm light for further processing. The remaining path of the 355 nm signal is similar to that of the 532 nm signal. The light is directed to a beam-splitter by a mirror, 1 % is transmitted for low altitude detection and 99 % is reflected toward the shutter for high altitude detection. Two plano-convex lenses focus the light onto the shutter's surface and collimate the light after the shutter. The 355 nm light is then focused at a point behind the detectors surface to fully illuminate the detector's surface area. Figure 13 shows a schematic drawing of the detector section. All the optical components are illustrated with the marginal ray paths through them. It should be noted that light never remains completely collimated as shown in Figure 13, and that some light may over fill the lenses and filters, thereby causing the system to be less efficient then expected. Appendix B lists all the optical components and their corresponding specifications.

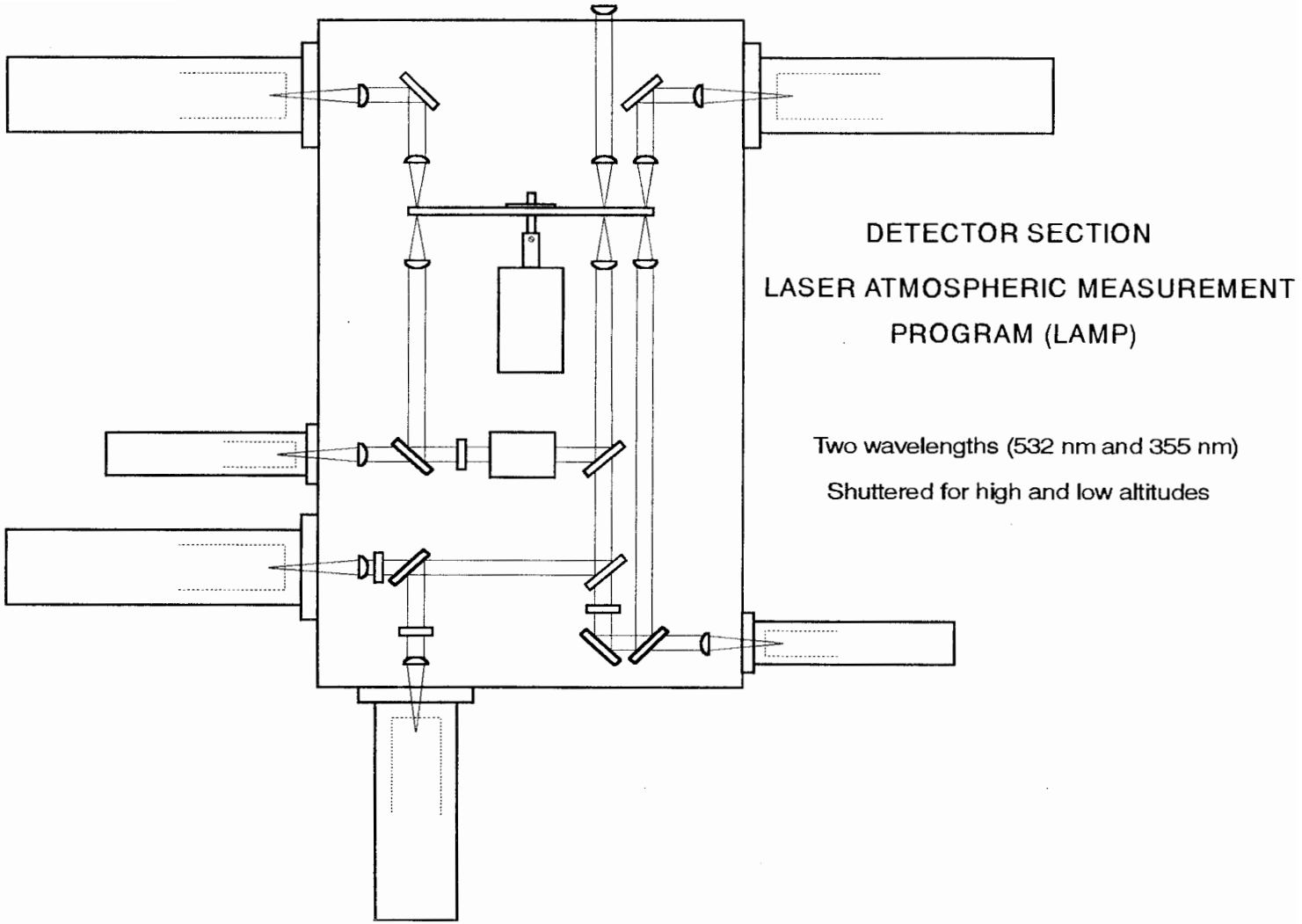

Figure 13. Schematic drawing of the detector section for the LAMP lidar.

4.2 Light Detection

The light detection converts the light signals to electrical signals so they can be recorded by the computer. The most common type of photodetector used in lidar systems is the photomultiplier tube (PMT). A PMT has an active area called a cathode that emits electrons when photons are incident on its surface. The electrons then interact with a series of dynodes that emit many electrons for every electron that contacts its surface. An avalanche is created that theoretically produces millions of electrons for every photon incident on the cathode. However, these detectors do have a limited quantum efficiency that is a function of the wavelength. Figure 14 shows a chart of quantum efficiency versus wavelength for a standard PMT. As can be seen from this chart PMT's are typically more efficient in the ultraviolet than in the infrared. One difficulty with PMT's is that they emit a current even when light is not incident on the cathode; this is called dark current and enters the data as background noise. Dark current can be decreased by cooling the PMT to -30° C with a thermoelectric cooled housing.

Three types of PMT's are used in the LAMP detector. The high altitude 532 nm channel and both Raman channels use Thorn EMI 9863B/350 photomultiplier tubes and are cooled to -30° C. These three channels receive very low levels of light and therefore are configured to count photons. These PMT's must respond very fast and be very efficient. The efficiencies of the PMT's to 532, 607, and 660 nm are 20, 7, and 5 % respectively. The 355 nm high altitude channel also receives a low level of light and its PMT, Thorn EMI 9893B/350, is also operated in photon counting mode. A different

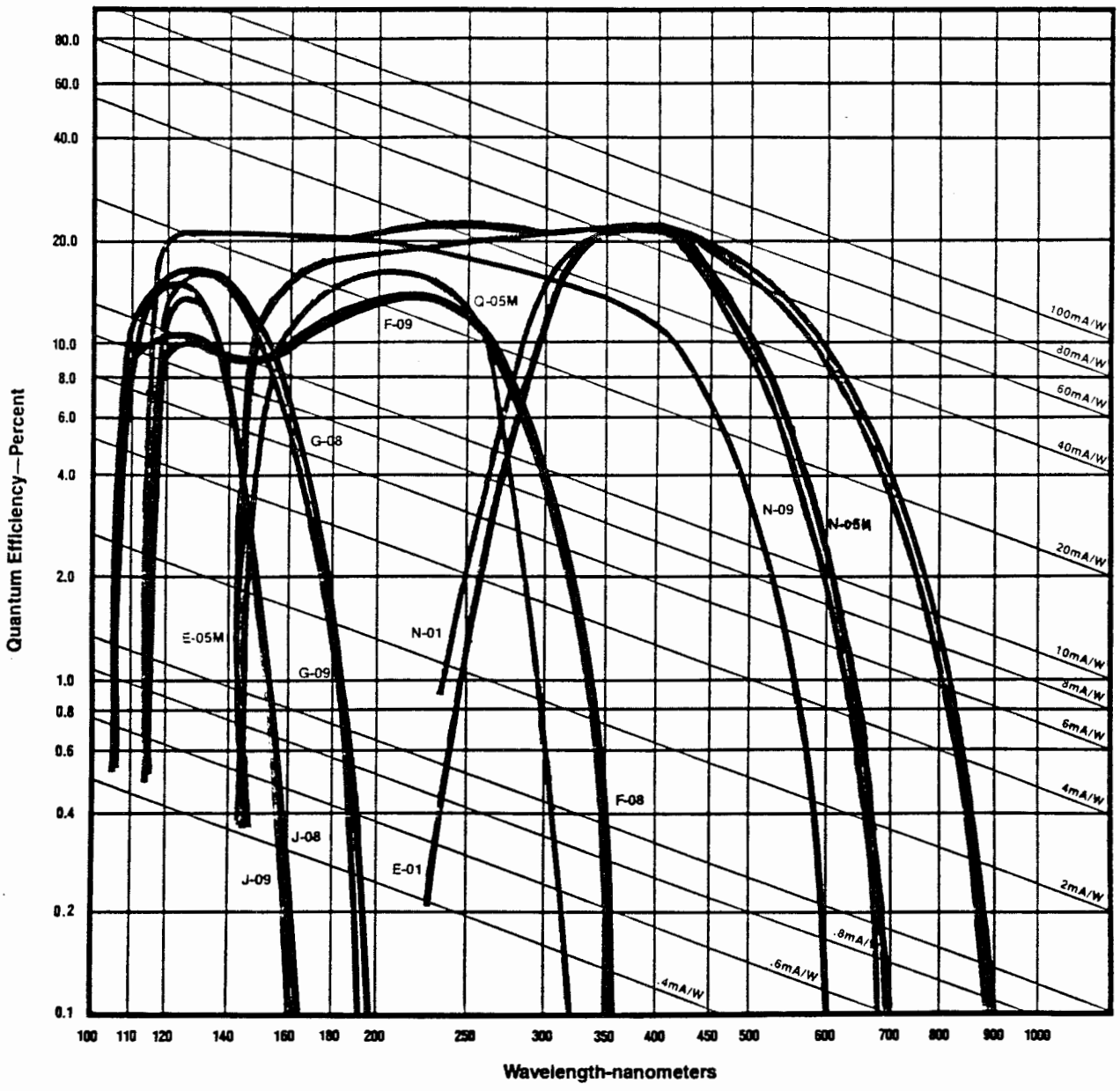

Figure 14. Typical spectral response characteristics for various photocathode materials in photomultiplier tubes. The PMT's are very inefficient in the infrared so dark current becomes an important factor. (Following the data sheet of EMR Schlumberger 1990.)

PMT was chosen for the 355 nm channel because a higher gain cathode material is available which reaches 24 % quantum efficiency in the ultraviolet. A third type of PMT, Thorn EMI 9828B03, is used for the greater light levels from the lower altitudes, which is cheaper but less efficient. The 355 and 532 nm low altitude channels receive much more light than do the other channels so quantum efficiency and dark current are not as important. Because of the greater light levels photon counting is not necessary, the current from the PMT's is converted to a voltage and digitized after a time constant of 200 nsec is added to the base signal.

The electrical signals from the photodetectors are then averaged for one minute intervals and recorded to WORM optical disks. The following section will present a few results of data obtained with this instrument along with some scientific explanations of the measurements.

Chapter 5

RESULTS

In this section several examples of data will be used to illustrate the capabilities of the LAMP lidar. Figure 15 shows a plot of raw photon counts and background noise versus altitude from the 355 nm high altitude channel, which was collected aboard the RV Polarstern on December 3, 1991, during a 30 minute average with a range resolution of 75 m. From this plot it can be seen that the shutter is fully open by 16 km. The background shown in this plot is 14 times larger than the actual background, because it is sampled 14 times for every one laser shot to improve the background noise statistics. Thousands of profiles like this one were obtained during the LADIMAS campaign to map the atmosphere as the RV Polarstern sailed between 70° N and 65° S. The data in Figure 16 were collected during the same run as the previous raw data except it is from the 532 nm channel. Here background noise was subtracted, the signal has been R^2 corrected, and then the ratio to the U.S. Standard Atmosphere was obtained. Taking the ratio to the U.S. Standard Atmosphere allows small perturbations in the density structure to be seen. Figure 17 shows a mean night temperature profile from the 355 nm data collected on 12/13/91. The temperature was calculated using the hydrostatic equation and integrating the density downward starting at high altitudes. The temperature converges within one and a half density scale heights (about 10 km) given some assumed initial value T_1[16]. The U.S Standard Atmosphere temperature is plotted along with the lidar temperature to provide a reference. Error bars indicate the statistical error of the measurement after the

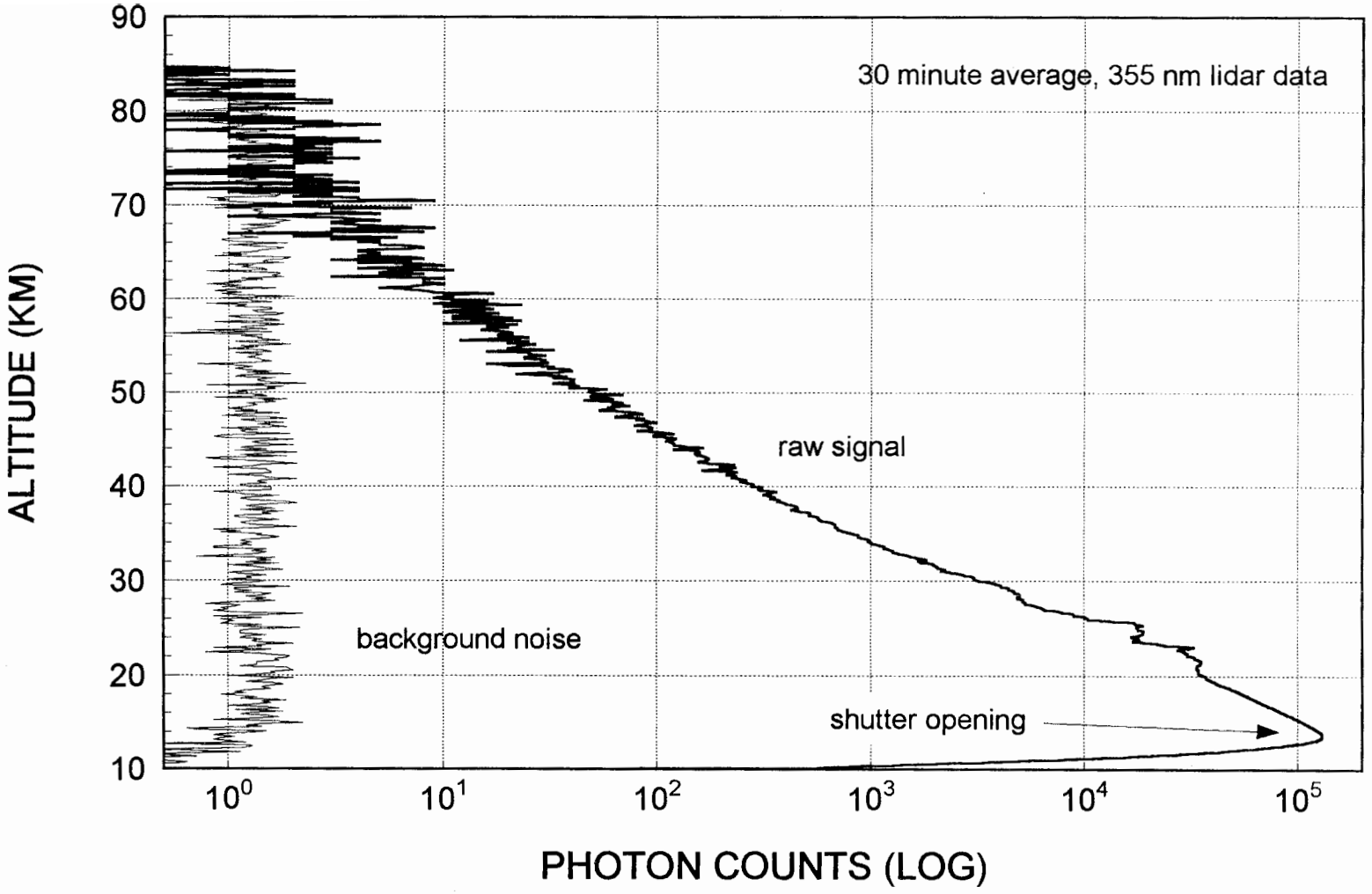

Figure 15. Raw photon counts collected 25 degrees south of the equator during the Ladimas campaign.

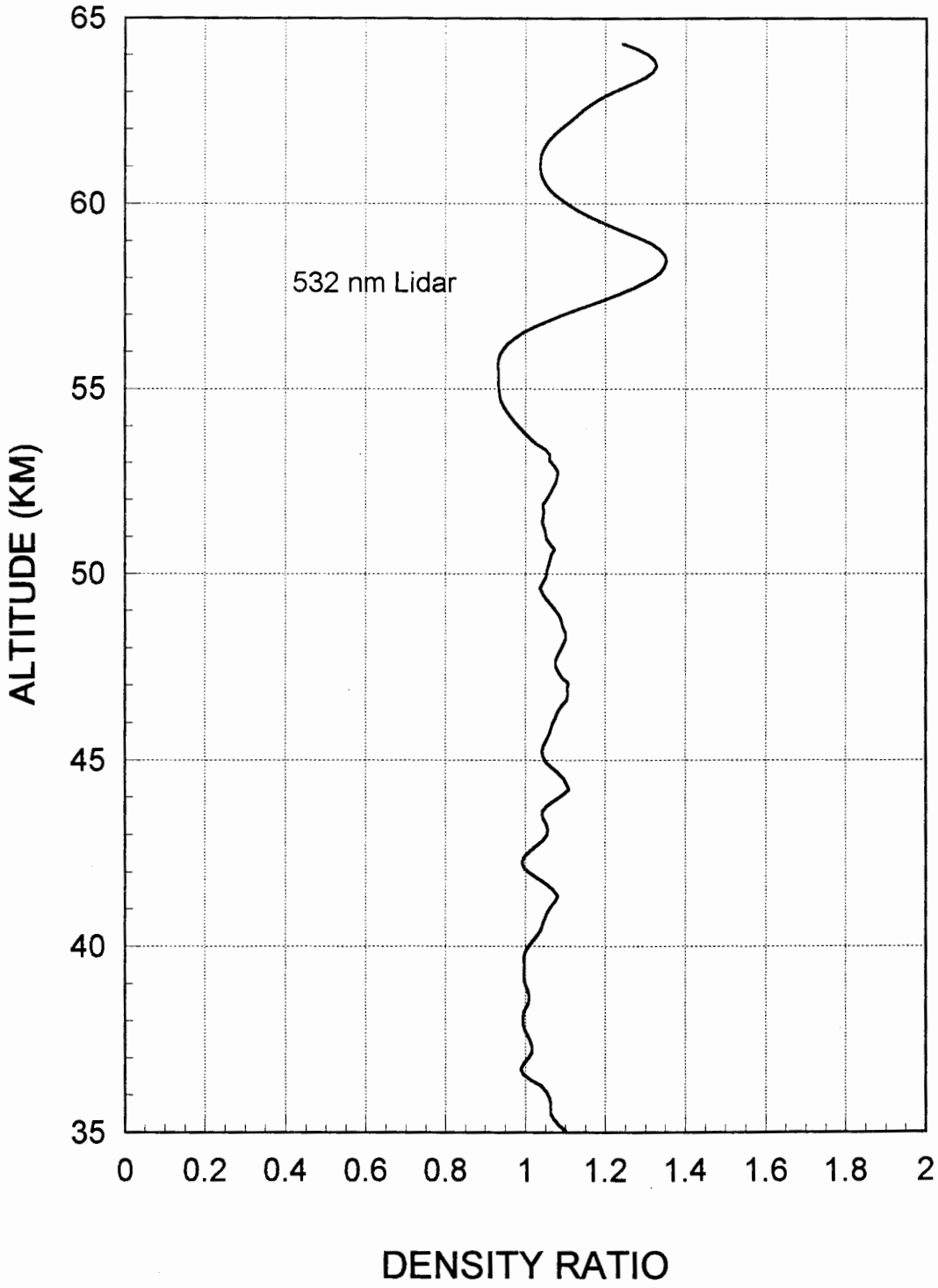

Figure 16. A 30-minute average density ratio to the US Standard collected on the RV Polarstern on the night of 12/03/91. .

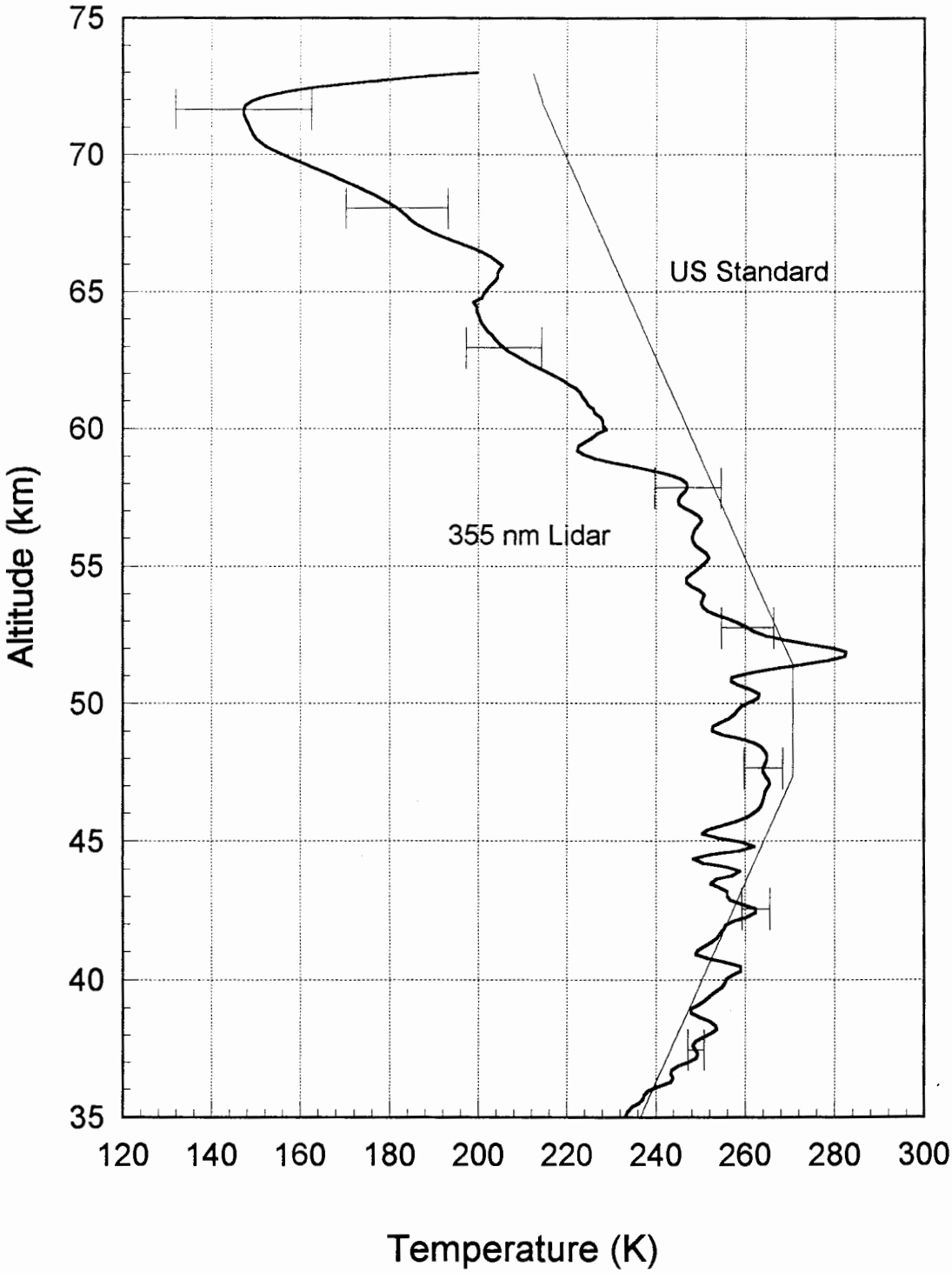

Figure 17. Mean night (150-min average) temperature profile obtained during the LADIMAS campaign aboard the RV Polarstern on 12/13/91.

data have been smoothed.

Scattering effects can be seen from stratospheric aerosols, which have been enhanced because of the Pinatubo volcano eruption in the Philippines; see Figure 15 between 20 and 30 km[9]. Due to the aerosols, the temperature and density ratio can only be calculated assuming molecular scattering above 30 km. By using the two-color measurements, the molecular scatterers can be distinguished from the particle components [17,18]. Figure 18 shows the information gathered on all channels for one 30 minute run. In this case, the similarity in the scattering from the stratospheric particles for the 355 and 532 nm wavelengths is obvious. A cirrus cloud appears as a large backscatter return at 10 km on the 532 nm channel, while it is barely noticeable on the 355 nm channel. The Raman N_2 profile contains scattering from only molecular nitrogen as can be seen in Figure 18. The particle backscattering peaks in the 355 and 532 nm channels indicate the concentration and size of the particles, while the Raman 607 nm return only indicates molecular nitrogen density and beam loss due to extinction. The Raman 607 nm profile would contain the true molecular density (78%) of the atmosphere, if it were not for the extinction from the laser beam due to the particle scattering. Between the 355 and 532 nm channels the extinction of the laser beam can be derived. Therefore, all the information needed to extend molecular temperature and density down through the troposphere is contained in Figure 18 with the 355, 532, and 607 nm profiles.

Also shown in Figure 18 is the 660 nm water vapor return, which is Raman shifted from 532 nm to 660 nm. The ratio of 660 nm to the 607 nm nitrogen return provides a direct measure of water vapor mixing ratio [15]. Because both the 607 and 660 nm

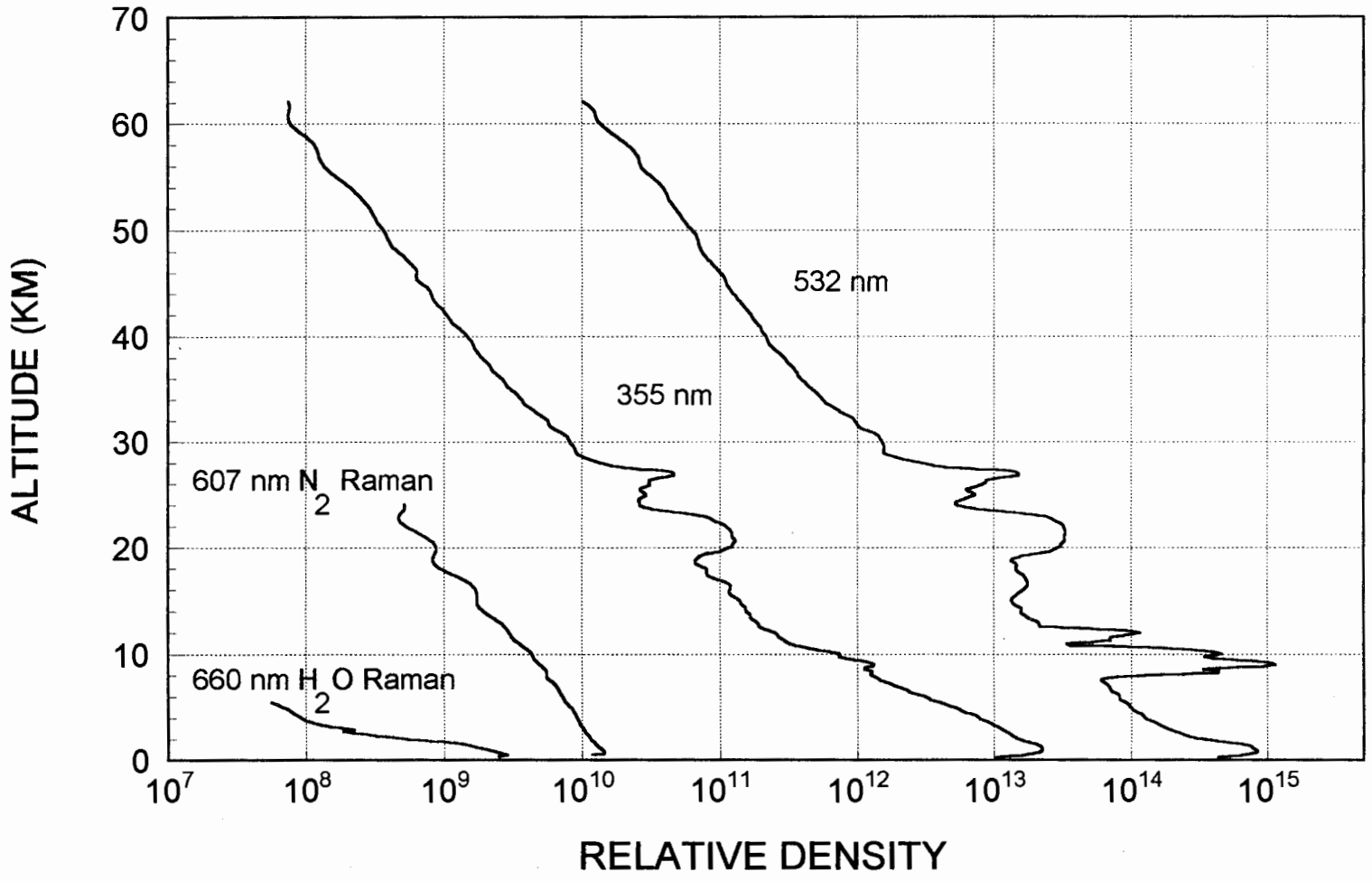

Figure 18. All six LAMP lidar profiles collected during a 30-minute average on 11/22/91. The 532 and 355 nm profiles were obtained by combining both the low and high altitude channels.

channels are part of the same instrument, the ratio does not need to be calibrated or tied off with any absolute measurement of the water vapor mixing ratio. These results show the value of lidar as a meteorological tool that will eventually replace standard weather balloons for lower atmospheric temperature and water vapor mixing ratios[12]. The data base collected during the LADIMAS campaign, along with the experience of continuously operating the lidar, is being used to develop a next generation lidar that will provide weather balloon type information without the use of costly disposable equipment.

Chapter 6

CONCLUSION

The LAMP instrument was designed as a research instrument capable of monitoring both the middle and lower atmosphere in almost any weather condition, a feature unique to this lidar. Six separate detector channels were needed to observe all the atmospheric variables required to extend lidar measurements through the troposphere and to the ground. Aerosol and cloud extinction as well as molecular nitrogen concentration have been measured to derive molecular temperature in the lower atmosphere. All these parameters complicate the optical design and engineering of the system. Each wavelength that must be detected adds additional beam-splitters, narrow band-pass filters, and lenses that in turn may decrease the overall efficiency of the instrument. Careful design and special coatings were used on all lenses and mirrors to minimize the loss of light signal through the system. Broader altitude ranges require more optical shuttering to measure through such a large dynamic range. In Chapter 3, it was shown that the backscattered return was shuttered twice in the LAMP lidar, once for 0 - 20 km and once for 16 - 80 km.

Results collected aboard the RV Polarstern as part of the LADIMAS campaign were presented in Chapter 5 to illustrate the capabilities of the LAMP instrument. These results demonstrated that the instrument could operate in all weather conditions and at sea. Many parameters over a wide range of altitudes were shown in Figure 18. The lessons learned from designing and building the optical detection system of LAMP are already

being used in the development of a smaller, more portable, fully automated future generation lidar. Data collected during the LADIMAS campaign is providing insight into the distribution of aerosols ejected into the stratosphere by one of the largest observed volcano eruptions. The Raman nitrogen and two-color lidar profiles obtained during the campaign are already helping to solve the problem of extending molecular temperature through the particle scatterers in the lower troposphere. All these examples show that the scientific goals were met in the optical design of the LAMP instrument.

REFERENCES

1. M. Alpers, J. Höfner, and U. von Zahn, "Iron atom densities in the polar mesosphere from lidar observations," *Geophysical Research Letters*, vol. 17, No. 12, pp. 2345-2348, 1990.

2. G. W. Bethke, R. L. Franklin, L. W. Springer, C. R. Philbrick, and J. P. McIsaac, "Ground-based lidar for upper atmospheric densities," *Proceedings of the Fifteenth International Symposium on Remote Sensing of Environment*, pp. 1007-1016, 1981.

3. M. R. Bowman, A. J. Gibson, and M. C. W. Sandford, "Atmospheric sodium measured by a tuned laser radar," *Nature*, vol. 221, p. 456, 1969.

4. M. L. Chanin, and A. Hauchecorne, "Lidar studies of temperature and density using Rayleigh scattering," *Middle Atmosphere Program Handbook for MAP*, vol. 13, pp. 87-98, 1984.

5. J. A. Cooney, "Measurements on the Raman component of laser atmospheric backscatter," *Applied Physics Letters*, vol. 12, No. 2, pp. 40-42, 1968.

6. L. Elterman, "The measurement of stratospheric density distribution with the searchlight technique," *Geophysical Research Papers*, No. 10, 48 pages, 1951.

7. J. C. Farman, B. G. Gardiner, and J. P. Shanklin, "Large losses of total ozone in Antarctica reveal seasonal ClO_x /NO_x interaction," *Nature*, vol. 315, pp. 207-210, 1988.

8. C. S. Gardner, D. G. Voelz, C. R. Philbrick, and D. P. Sipler, "Simultaneous lidar measurements of the sodium layer at the Air Force Geophysics Laboratory and The University of Illinois," *Journal of Geophysical Research,* vol. 91, No. A11, 1986.

9. G. P. Gobbi, F. Congeduti, and A. Adriani, "Early stratospheric effects of the Pinatubo eruption," *Geophysical Research Letters*, vol. 19, No. 10, pp. 971-1000, 1992.

10. E. Hecht, *Optics*. Massachusetts: Addison-Wesley Publishing Company, 1987.

11. P. Juramy, M. L. Chanin, G. Megie, G. F. Toulinov, and Y. P. Doudoladov, "Lidar sounding of the mesospheric sodium layer at high latitude," *J. Atmos. Terr. Phys.*, vol 43, No. 3. pp. 209-215, 1981

12. M. P. McCormick, "The use of lidar for atmospheric measurements," *In Remote Sensing Energy Related Studies*, Washington: Hemisphere Press, 1975.

13. R. M. Measures, *Laser remote sensing*. New York: John Wiley & Sons, 1984.

14. S. H. Melfi, J. D. Lawrence, Jr., and M. P. McCormick, "Observation of Raman scattering by water vapor in the atmosphere," *Applied Physics Letters*, vol. 15, No. 9, pp. 295-297, 1969.

15. S. H. Melfi, D. Whiteman, and R. Ferrare, "Observation of atmospheric fronts using Raman lidar moisture measurements," *Journal of Applied Meteorology*, vol. 28, pp. 789-806, 1989.

16. C. R. Philbrick, F. J. Schmidlin, K. U. Grossman, G. Lange, D. Offerman, K. D. Baker, D. Krankowsky, and U. von Zahn, "Density and temperature structure over northern Europe," *J. Atmos. Terr. Phys.*, vol. 47, pp. 159-172, 1985.

17. C. R. Philbrick, D. P. Sipler, G. Davidson, and W. P. Moskowitz, "Remote sensing of structure properties in the middle atmosphere using lidar," *Proceedings of OSA Meeting on Laser and Optical Remote Sensing*, pp. 120-123, 1987.

18. C. R. Philbrick, D. P. Sipler, B. E. Dix, G. Davidson, W. P. Moskowitz, C. Trowbridge, R. Sluder, F. J. Schmidlin, L. D. Mendenhall, K. H. Bhavnani, And K. J. Hahn, "Measurements of the high latitude middle atmosphere properties using LIDAR," *AFGL-TR-87-0053, Environmental Research Papers*, no. 967, Geophysics Laboratory, 129 pages, 1987.

19. C. R. Philbrick, D. B. Lysak, T. D. Stevens, P. A. T. Haris, and Y. -C. Rau, "Atmospheric Measurements Using the LAMP lidar during the LADIMAS campaign," *Proceedings of the 16th International laser Radar Conference*, to be published, 1992.

20. H. Shimizu, Y. Sasano, H. Nakane, N. Sugimoto, I. Matsui, and N. Takeuchi, "Large scale laser radar for measuring aerosol distribution over a wide area," *Applied Optics*, vol. 24, no. 5, pp. 617-626, 1985.

21. T. Slingo, "Wetter clouds dampen global greenhouse warming," *Nature*, vol. 341, p. 104, 1989.

Appendix A

CIRCUIT DIAGRAMS

The following circuits control everything from the laser Q-switch to the data collection for the LAMP lidar. The circuits are divided into four sections: shutter trigger timing logic, low altitude channel, high altitude channel, and Raman channel. The shutter trigger timing logic counts shutter triggers and controls the 16 shutter opening cycle discussed in Chapter 3. This circuit section also sends the flash lamp and Q-switch signals to the laser. Triggers are then sent to the low altitude, high altitude, and Raman channels to initiate data collection. The low altitude, high altitude, and Raman channel circuit sections send the proper triggers to either photon counting modules or digitizing modules to collect data. These units have to be controlled to start data collection, end data collection, and shift the data to an averager. The position of the data in memory is also controlled by the circuits. The 14 background samples are placed in the first 4000 bytes of memory, the single laser shot is placed in the next 4000 bytes, and the energy monitor data is stored in the last 182 bytes of memory.

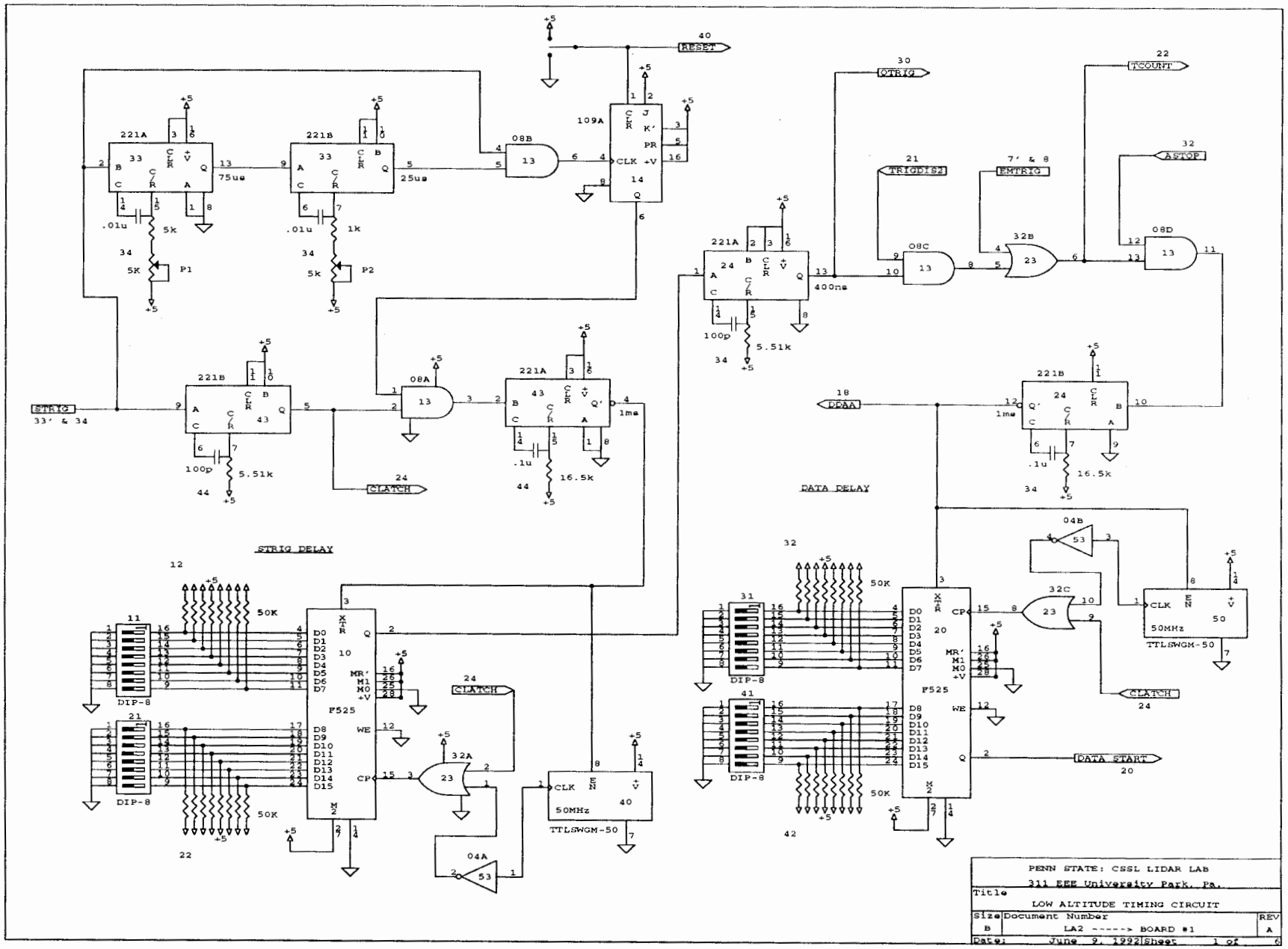

Figure 19. Low altitude timing circuit, shutter trigger section.

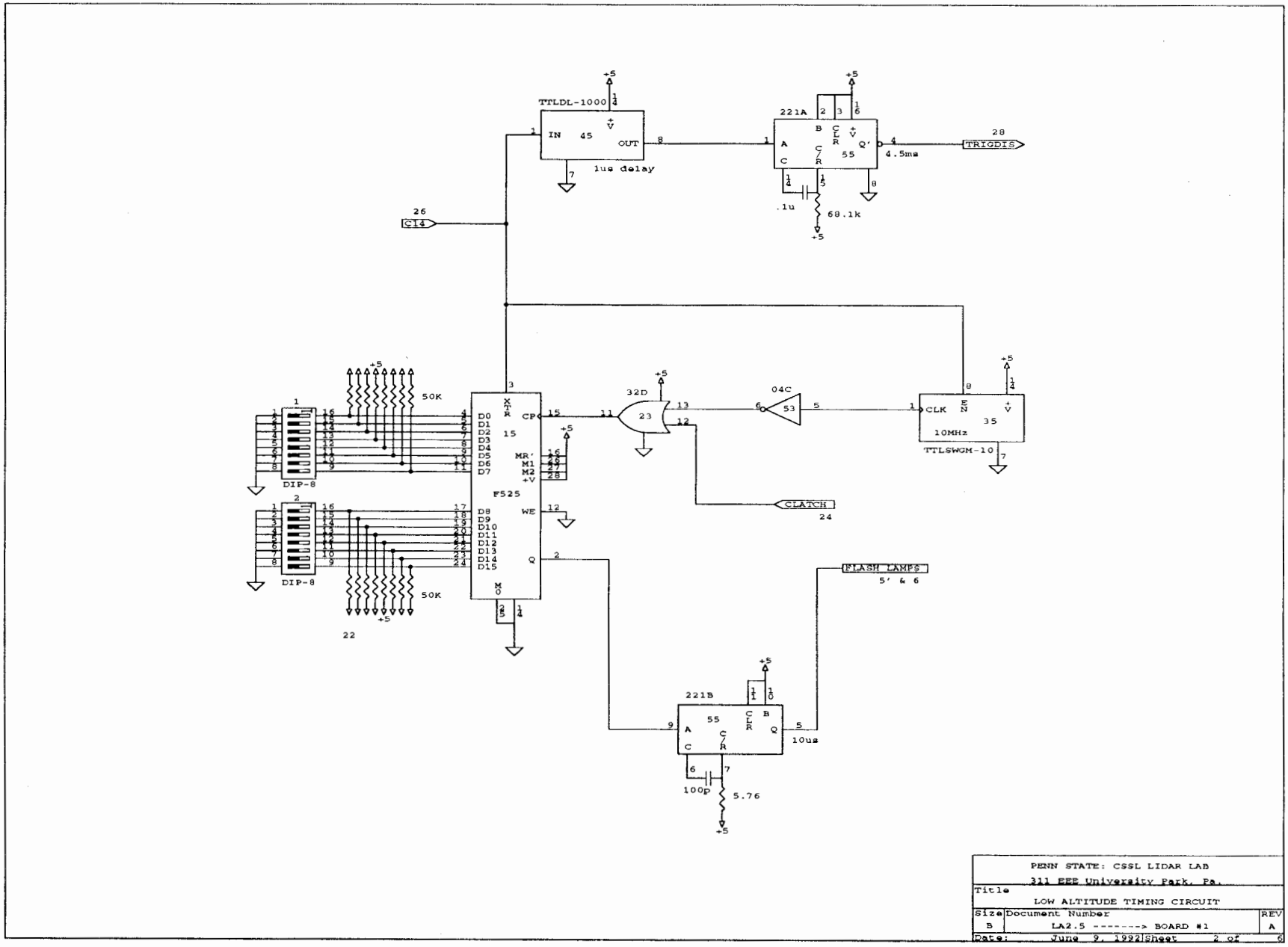

Figure 20. Low altitude timing circuit, laser flash lamp section.

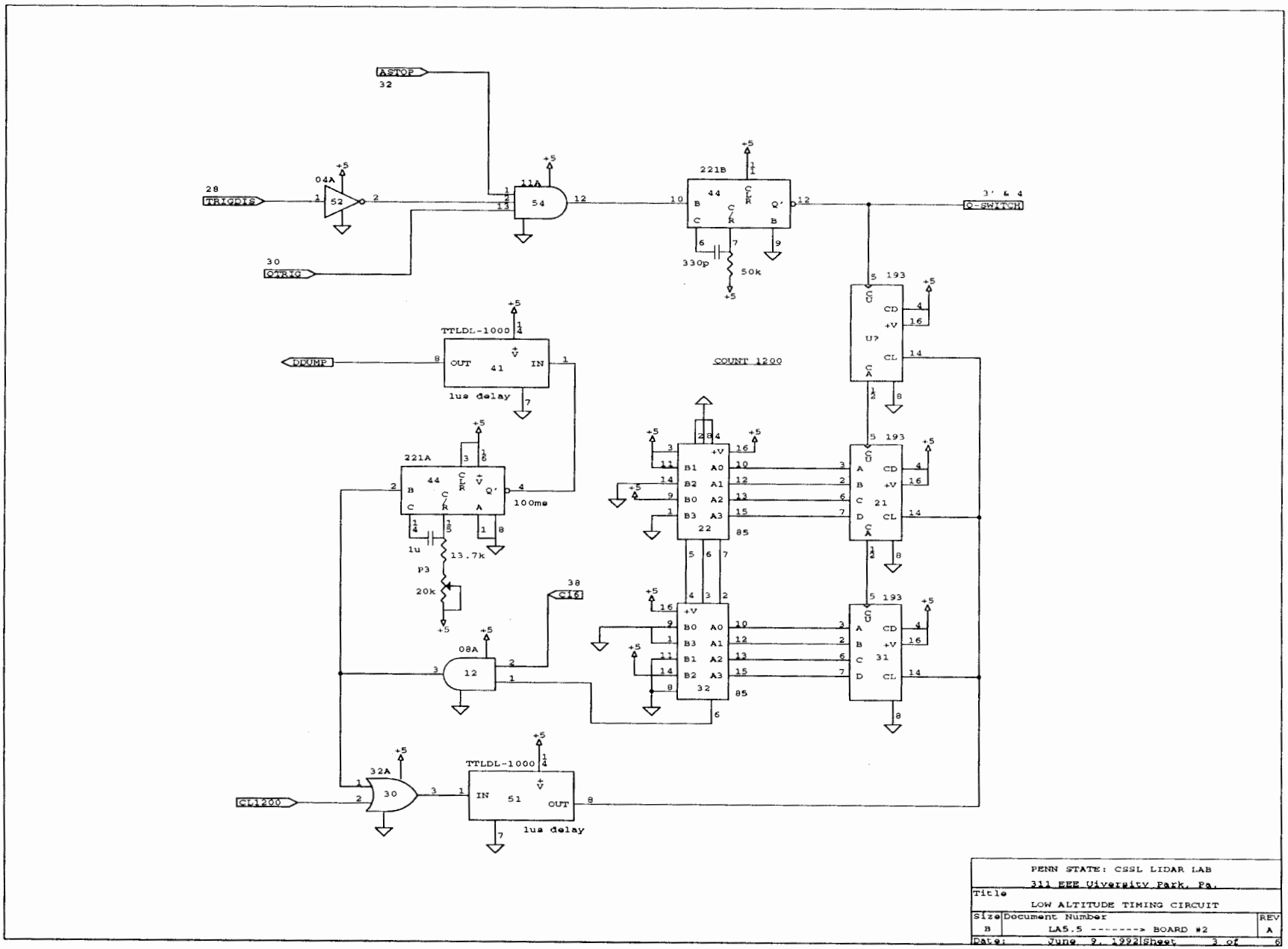

Figure 21. Low altitude timing circuit, laser Q-switch section.

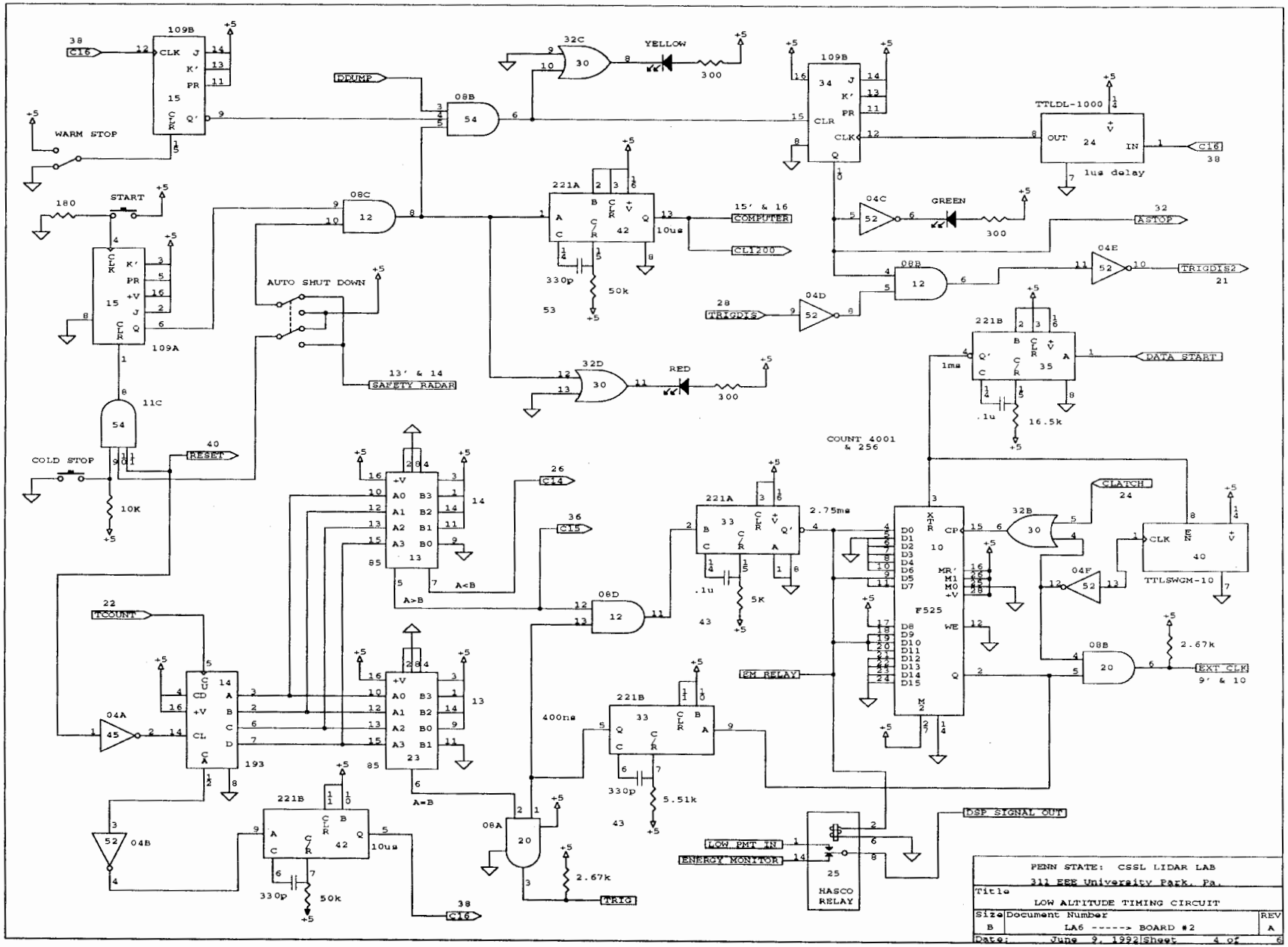

Figure 22. Low altitude timing circuit, data collection section.

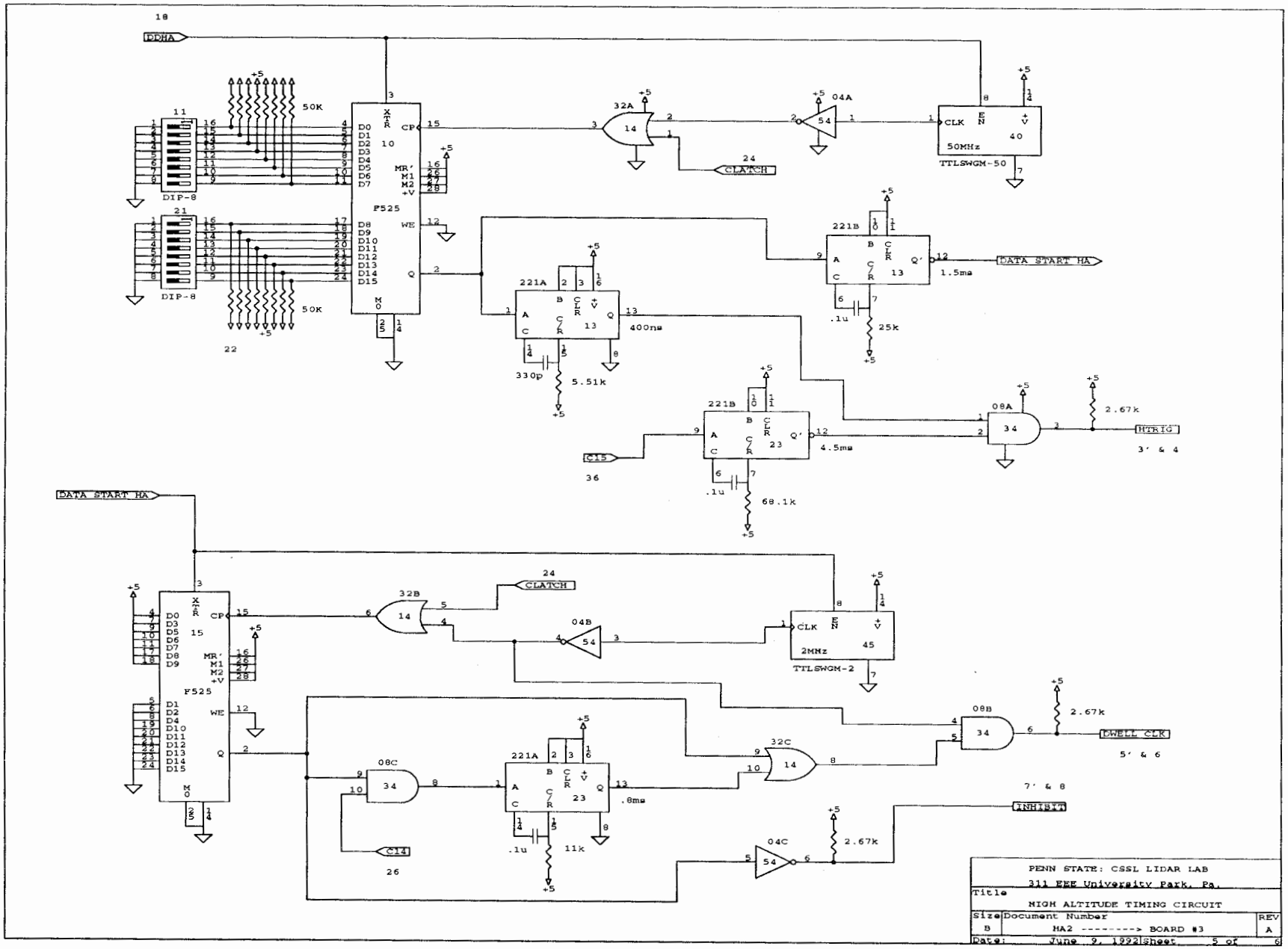

Figure 23. High altitude data collection timing circuit.

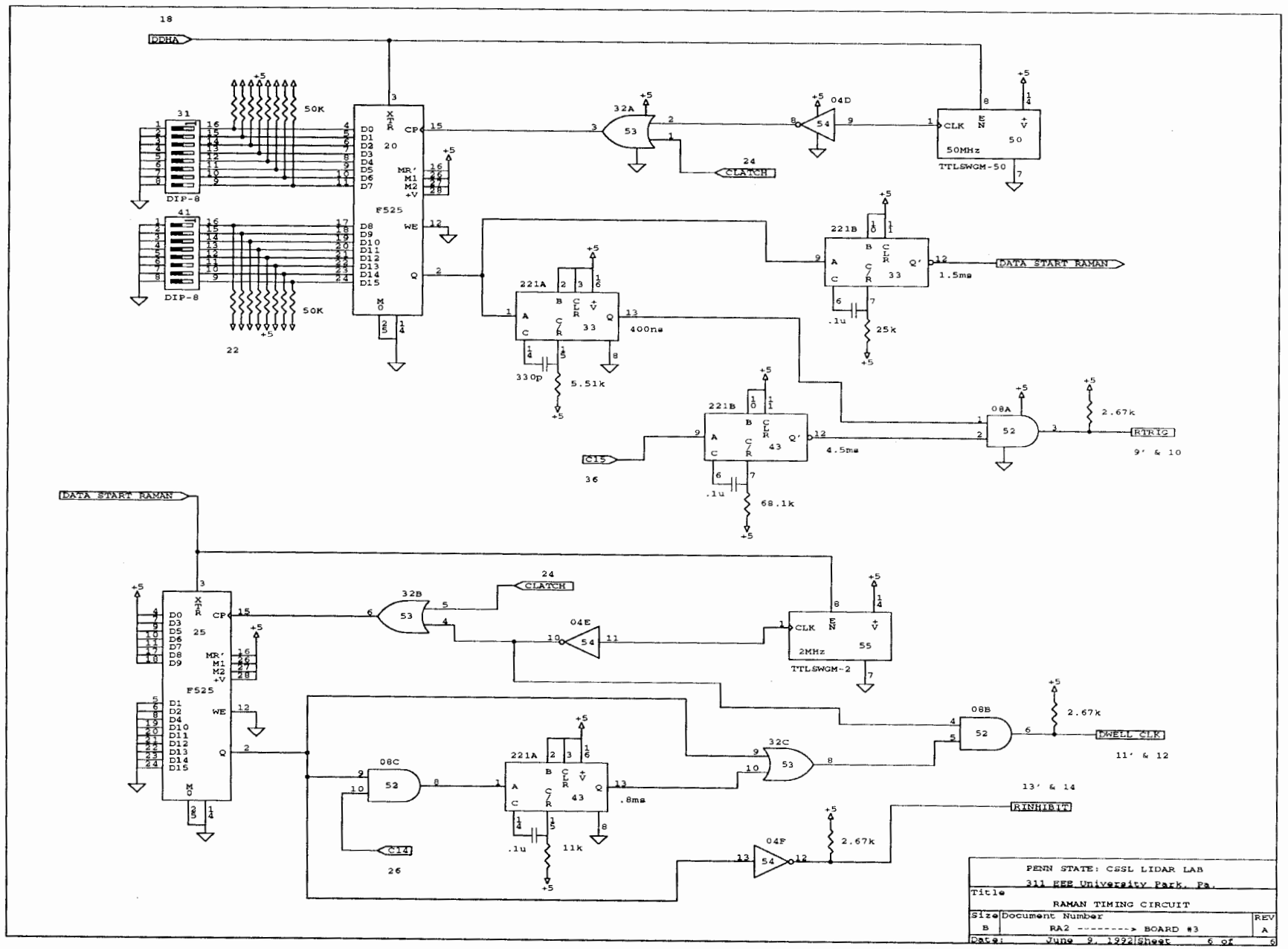

Figure 24. Raman channel data collection timing circuit.

Appendix B

DETECTOR BOX CONTENTS

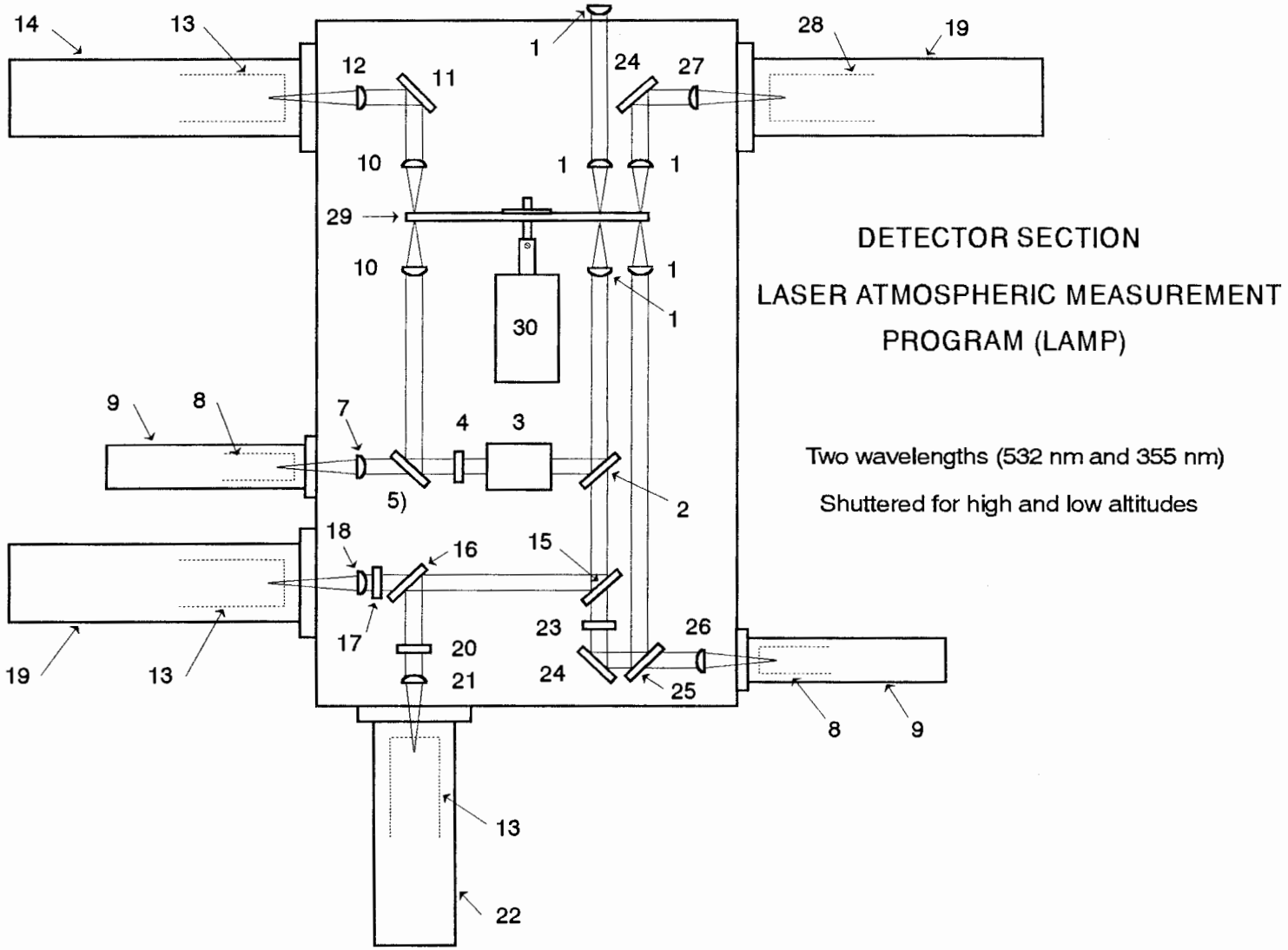

Figure 25. Schematic drawing of the detector section for the LAMP lidar.

Key for Figure 25

1) Fused silica plano-convex lens, d = 25.4 mm, F = 50.8 mm, AR coated for 355, 532, 607, and 660 nm.

2) Dichroic beam-splitter, d = 50.8 mm, reflects 99.5 % at 532 nm, transmits 82 % at 355 nm and 86 % at 607 and 660 nm.

3) Fabry-Perot etalon, electronically tuned to transmit 532 nm with a .01 nm bandwidth.

4) 532 nm narrow band-pass filter, temperature stabilized at 34° C, transmits 55 % at 532 nm with a .29 nm bandwidth.

5) 532 nm beam-splitter, transmits 1 %, reflects 99 %.

7) Glass plano-convex lens, d = 25.4 mm, F = 175 mm, AR coated for 532 nm.

8) 28 mm Thorn EMI 9828B03 PMT, digitized.

9) 28 mm Thorn EMI socket and housing assembly.

10) Glass plano-convex lens, d = 25.4 mm, F = 50.8 mm, AR coated for 532 nm.

11) 532 nm high reflectivity mirror, d = 50.8 mm, reflects 99.8 %.

12) Glass plano-convex lens, d = 25.4 mm, F = 200 mm, AR coated for 532 nm.

13) 52 mm Thorn EMI 9863B/350 PMT, photon counted.

14) 52 mm Thorn EMI thermoelectric cooled (- 25° C) PMT socket and housing assembly.

15) Dichroic beam-splitter, d = 50.8 mm, reflects 99.5 % at 607 and 660 nm, transmits 82 % at 355 nm.

16) Dichroic beam-splitter, d = 50.8 mm, reflects 99.5 % at 660 nm, transmits 85 % at 607 nm.

17) 607 nm narrow band-pass filter, transmits 83 % at 607 nm with a 3.5 nm bandwidth.

18) Glass plano-convex lens, d = 25.4 mm, F = 62.9 mm, AR coated for 607 nm.

19) Amherst Scientific thermoelectric cooled (- 30° C) PMT socket and housing assembly.

20) 660 nm narrow band-pass filter, transmits 83 % at 660 nm with a 3.5 nm bandwidth.

21) Glass plano-convex lens, d = 25.4 mm, F = 200 mm, AR coated for 660 nm.

22) Pacific Research thermoelectric cooled (- 25° C) PMT socket and housing assembly.

23) 355 nm narrow band-pass filter, transmits 24 % at 355 nm with a 3.2 nm bandwidth.

24) 355 nm high reflectivity mirror, d = 50.8 mm, reflects 99.8 %.

25) 355 nm beam-splitter, transmits 1 %, reflects 99 %.

26) Fused silica plano-convex lens, d = 25.4 mm, F = 175 mm, AR coated for 355 nm.

27) Fused silica plano-convex lens, d = 25.4 mm, F = 100 mm, AR coated for 355 nm.

28) 52 mm Thorn EMI 9893B/350 PMT, photon counted.

29) Aluminum high speed (4800 rpm) optical chopper wheel, d = 10 inches.

30) Hysteresis synchronous motor for chopper wheel.